NASA Technical Paper 2781

1988

Advances in Contact Algorithms and Their Application to Tires

Ahmed K. Noor
The George Washington University
Joint Institute for Advancement of Flight Sciences
Langley Research Center
Hampton, Virginia

John A. Tanner
Langley Research Center
Hampton, Virginia

National Aeronautics
and Space Administration

**Scientific and Technical
Information Division**

Contents

Summary

Currently used techniques for tire contact analysis are reviewed. Discussion focuses on the different techniques used in modeling frictional forces and the treatment of contact conditions. A status report is presented on a new computational strategy for the modeling and analysis of tires including solution of the contact problem. The strategy is based on solving the complex tire contact problem as a sequence of simpler problems and obtaining information about the sensitivity of the tire response to each of the complicating factors.

The key elements of the proposed strategy are (1) use of semianalytic finite elements in which the shell variables are represented by Fourier series in the circumferential direction and piecewise polynomials in the meridional direction, (2) use of perturbed Lagrangian formulation for the determination of the contact area and pressure, (3) application of multilevel operator splitting to effect successive simplifications of the governing equations, and (4) application of multilevel iterative procedures and reduction techniques to generate the response of the tire.

The tire variables include strain components, stress resultants, and generalized displacements, with the strain components and stress resultants allowed to be discontinuous at interelement boundaries. The perturbed Lagrangian formulation results in a better conditioning of the equations to be solved and in reducing the number of iterations required in the solution process. Multilevel operator splitting is used to uncouple the equations associated with different harmonics, to identify the effects of different Fourier harmonics, to delineate the effect of nonorthotropic material properties on the response, and to identify regions in which more sophisticated mathematical and/or computational models are needed. Reduction techniques allow substantial reduction in the total number of degrees of freedom used in generating the response of the tire. Multilevel iterative procedures include nested applications of the preconditioned conjugate gradient (PCG) technique. The PCG technique provides a stable and rapidly convergent iterative procedure. Numerical results are presented to demonstrate the effectiveness of a proposed procedure for generating the tire responses associated with different Fourier harmonics.

Symbols

E_L, E_T	elastic moduli in direction of fibers and normal to it
$\{E\}_n$	vector of strain parameters associated with the nth Fourier harmonic for the tire (see eqs. (10) and table 1)
$\{f\}^{(0)}, \{f\}^{(1)}, \ldots \{f\}^{(N)}$	vectors defined in eqs. (8)
G_{LT}, G_{TT}	shear moduli in the plane of fibers and normal to it
$\{G\}^{(n)}$	vector of nonlinear terms associated with the nth Fourier harmonic (see eqs. (8))
$\{H\}_n$	vector of stress-resultant parameters, associated with the nth Fourier harmonic, for the tire (see eqs. (10) and table 1)
h	total thickness of the tire
$[K]^{(n)}$	linear matrix associated with the nth Fourier harmonic (see eqs. (8))
$[\tilde{K}], [\hat{K}]$	matrices defined in equations (9)
$[K_o], [K_a]$	submatrices of $[K]^{(n)}$ (see eqs. (11))
$[K]^{(IJ)}$	matrices containing nonlinear terms (see eqs. (12) and (14))
$[\tilde{k}], [\hat{k}]$	matrices associated with the reduced equations (see eqs. (18), (19), and (20))
$M_s, M_\theta, M_{s\theta}$	bending and twisting stress resultants (see fig. 2)
N	number of Fourier harmonics which are greater than or equal to one
$N_s, N_\theta, N_{s\theta}$	extensional stress resultants (see fig. 2)

N^i	shape functions used in approximating the generalized displacements and external loading
$N^{i'}$	shape functions used in approximating the stress resultants and strain components
n	Fourier harmonic (circumferential wave number)
n_o	Fourier harmonic at which global approximation vectors are generated
p_o	intensity of localized normal loading on the tire (see figs. 2 and 4)
p_n	normal pressure components associated with the nth Fourier harmonic
p_s, p_θ, p	intensity of external loading in the coordinate directions (see fig. 2)
$\{P\}, \{\hat{P}\}$	right-side vectors in equations (16)
$\{P\}^{(n)}$	consistent load vector, associated with the nth Fourier harmonic, for the tire (see eqs. (8))
Q_s, Q_θ	transverse shear stress resultants (see fig. 2)
$\{q\}, \{\hat{q}\}$	load vectors associated with the reduced equations (see eqs. (18), (21), and (22))
$[Q], [R]$	submatrices of $[K]^{(n)}$ (see eqs. (11))
$[S_o], [S]$	submatrices of $[K]^{(n)}$ (see eqs. (11))
s	meridional coordinate of tire (see fig. 2)
u, v, w	displacement components of the middle surface of the tire in the meridional, circumferential, and normal directions, respectively (see fig. 2)
U_n	total strain energy of the shell associated with the nth load harmonic p_n
$\{X\}_n$	vector of generalized nodal displacement coefficients for the tire (see eqs. (10) and table 1)
x_3	coordinate normal to the tire middle surface (see fig. 2)
$\{Z\}_n$	vector of unknowns associated with the nth Fourier harmonic
β	contact angle in meridional direction
$[\Gamma]$	matrix of global approximation vectors (see eqs. (17))
ε	penalty parameter
$\varepsilon_s, \varepsilon_\theta, 2\varepsilon_{s\theta}$	extensional strains of the middle surface of the tire
$2\varepsilon_{s3}, 2\varepsilon_{\theta 3}$	transverse shear strains of the tire
θ	circumferential (hoop) coordinate of the tire (see fig. 2)
$\kappa_s, \kappa_\theta, 2\kappa_{s\theta}$	bending strains of the tire
$\{\lambda\}_n$	vector of Lagrange multiplier parameters associated with the nth Fourier harmonic (see eqs. (10))
$\breve{\lambda}$	tracing parameter identifying the coupling between the different Fourier harmonics (see eqs. (15))

ν_{LT}	major Poisson's ratio of the individual layers
ξ	dimensionless coordinate along the meridian (see fig. 3)
ϕ_s, ϕ_θ	rotation components of the middle surface of the tire (see fig. 2)
$\{\psi\}_n$	vector of amplitudes of global approximation vectors (see eqs. (17))

Superscripts:

i	index of shape functions for approximating generalized displacements and external loadings; ranges from 1 to the number of displacement nodes
i'	index of shape functions for approximating stress resultants and strain components, ranges from 1 to the number of parameters to approximate each stress resultant and strain component
t	matrix transposition
$-$	coefficient of sine terms in Fourier series

Subscript:

max	maximum value

1. Introduction

Contact problems have occupied a position of special importance in tire mechanics because the contact area is where the forces are generated to support, guide, and maneuver the vehicle. The distributions of contact pressures and frictional forces define the moments and shears that are applied to the vehicle suspension system (ref. 1). Under rolling conditions, the distribution of sliding velocities within the tire footprint combined with the frictional force distribution defines the rate of energy dissipation for the tire and provides a measure of tire wear (refs. 2 and 3).

Modeling of the contact phenomena in the tire footprint is a formidable task due, in part, to the difficulty of modeling the tire response. Both the distribution of tractions and the footprint geometry are functions of the tire normal, frictional, and inflation loads. Moreover, the complex mechanisms of dynamic friction, which allow the tire to develop the necessary steering and braking forces for vehicle control, are not fully understood (ref. 4). The tire analyst thus is forced to choose among several friction theories. When the tire contact problem includes frictional effects, the solution becomes path dependent and uniqueness of the solution is not guaranteed.

The tire is a composite structure composed of rubber and textile constituents which exhibit anisotropic and nonhomogeneous material properties. Normal tire operating conditions create loads that can produce large structural rotations and deformations. Elevated operating temperatures, caused by combined effects of hysteresis and frictional heating, can cause variations in the material characteristics of the tire constituents (refs. 5–7). The laminated carcasses of aircraft tires are thick enough to allow significant transverse shear deformations.

The aforementioned facts and the attending difficulties can make the cost of tire analysis prohibitive. Hence, there is a need to develop modeling strategies and analysis methodologies, including contact algorithms, to reduce this expense. In recent years nonlinear analyses of static and dynamic problems involving contact have been the focus of intense research efforts. Novel techniques which have emerged from these efforts include semianalytic finite element models for the nonlinear analysis of shells of revolution (refs. 8 and 9), reduction methods (refs. 10 and 11), and operator splitting techniques (refs. 12–14).

Current research on tire modeling and analysis at NASA Langley Research Center is aimed at developing an accurate and cost-effective strategy for predicting the tire response. This is being accomplished by combining the aforementioned techniques with more recent developments in analysis methods, in particular the perturbed Lagrangian formulation (refs. 15 and 16) and iterative procedures based on the preconditioned conjugate gradient (PCG) technique (refs. 17–19), for the determination of the contact area and pressure distribution.

The objectives of this paper are (1) to review currently used techniques for tire contact analysis with particular emphasis on the modeling of frictional forces, (2) to present the status of an effective computational strategy for tire analysis including the solution of tire contact problems, and (3) to describe some experimental programs that are currently being used to develop a data base for verification of the analysis results.

2. Key Elements of Contact-Friction Problems

Contact-friction problems are inherently nonlinear and path dependent. The nonlinearity is due in part to the fact that both the contact area and the contact pressures are not known a priori and they vary during the load history. The path dependence is a result of the nonconservative (irreversible dissipative) character of the frictional forces.

The four key elements of contact-friction problems are (1) finite element formulation and model used, (2) modeling of frictional forces, (3) treatment of contact conditions and the numerical procedure used for updating these conditions, and (4) computational algorithm used which includes the iteration procedure, convergence criteria, and traction recovery. The discussion in this section focuses on both the frictional modeling and the contact conditions. In section 3 different methods for solution of contact problems are briefly reviewed.

2.1. Friction Models for Tires

Most of the existing literature on contact-friction problems deals with metal-to-metal contact (ref. 4). The major phenomenon associated with this class of problems is the plastic deformation of asperities within the contact zone. The frictional characteristics of the metal surfaces are generally assumed to be a function of surface roughness, the presence of surface films, and contact pressures, which are high enough to generate plastic flow of the asperities in the contact interface.

Problems associated with pneumatic tires form an important subset of contact-friction problems. For this set of problems the pressure in the contact region is a function of the tire inflation pressure (ref. 2). The presence of inflation pressure results in lower contact pressures in tires than those associated with metal-to-metal contact. For most combinations of tire and road surfaces, the frictional characteristics of the tire-pavement interface are influenced by the speed of the vehicle, surface roughness, and the presence of contaminants such as water, ice, or snow on the surface. However, in this section, only the static and low-speed test conditions on a dry surface are considered. Under these conditions the frictional characteristics of the tire-pavement interface are insensitive to variations in surface roughness and, therefore, are a function of the tire inflation pressure only (ref. 3).

A number of models have been developed in an effort to explain the phenomena associated with friction. These include (1) classical friction models and their various extensions, (2) adhesion-plowing models, and (3) nonlocal friction models.

2.1.1. Classical models. The first group of models, classical friction models, was first presented by Amontons in 1699 and extended by Coulomb in 1781. These models were developed to describe the gross motions of effectively rigid bodies in contact. The frictional force at the onset of, and during, sliding is proportional to the normal contact force. This is described by the familiar relation:

$$|T_u| = \mu T_n \tag{1}$$

where T_u and T_n are the frictional and the normal forces, respectively, and μ is the coefficient of friction. The following assumptions are generally made with regard to the coefficient of friction and the direction of the frictional force:

1. The coefficient of friction is independent of both the apparent area of contact and the sliding velocity.
2. The frictional force acts in the slide direction of the relative tangential velocity but in opposite sense.

Experiments have shown that the first assumption generally is not valid. In fact, the static coefficient of friction at the onset of sliding μ_s is greater than the dynamic coefficient during sliding μ_a. However, for limited velocity ranges, the variation of μ with velocity can be neglected. The second assumption regarding the direction of the frictional force is a reasonable approximation for surfaces without pronounced directional properties. However, the frictional force may change direction continuously as sliding proceeds.

2.1.2. Adhesion-plowing models. Tabor (ref. 20) has proposed the adhesion-plowing theory of friction. This theory suggests that the coefficient of friction is the sum of two components:

$$\mu = \mu_a + \mu_p \tag{2}$$

where μ_a is the adhesion friction component and μ_p is the plowing friction component. In its simplest form the adhesion component of friction is as follows:

$$\mu_a = \tau / H \tag{3}$$

where τ is the shear strength of the softer contacting material and H is the hardness of the softer contacting material.

The adhesion component of friction is compatible with the classical laws of friction and leads to frictional forces that are proportional to the normal load and independent of the area of contact. The plowing component of friction can be modeled as a hard conical asperity grooving a softer surface. For

most engineering applications, however, the plowing component of friction is assumed to be negligible.

Both classical friction laws and adhesion-plowing theory lead to solution algorithms which do not guarantee unique solutions for contact-friction problems, friction being a dissipative process and, therefore, leading to path-dependent solutions.

2.1.3. Nonlocal friction models. The third type of friction models, the nonlocal models (such as the one proposed by Oden and Pires, ref. 21), account for the microscopic aspects of the physics of friction. Despite their elegance, the characterization of these models for practical situations is still a problem. Moreover, uniqueness of solution is guaranteed only for a sufficiently small friction coefficient.

Examination of the various friction models currently in use suggests that the classical friction models are adequate for use in tire contact problems. However, these models need to be modified slightly to incorporate the influence of inflation pressure on the friction characteristics of the tire-pavement interface.

2.2. Analogy Between Frictional Behavior and Elastoplastic Response

Although specific details may differ significantly, an analogy exists between frictional behavior and elastoplastic response of solids. The following elements of frictional behavior (on left) correspond to the indicated elements of elastoplastic behavior of solids (on right):

Dry friction	$\longleftrightarrow$	Elastic-rigid plastic response
Frictional sliding	$\longleftrightarrow$	Nonassociated plasticity (e.g., for granular materials)
Slip surface	$\longleftrightarrow$	Yield surface
Static coefficient of friction during slip	$\longleftrightarrow$	Strain hardening
Directional dependence (anisotropic) friction behavior	$\longleftrightarrow$	Anisotropic plasticity

This analogy is useful in applying the efficient numerical algorithms developed for the elastoplastic problems to contact-friction problems.

2.3. Contact Conditions

On the contact surface, the following conditions must be satisfied:

1. No gap or penetration of material points occurs at the place of contact.
2. Normal tractions at contact points are compressive.
3. Relative sliding occurs when the tangential traction reaches the value of the normal traction times the coefficient of friction.
4. During sliding, the tangential traction component is related to the tangential displacement component and counteracts the relative movement of the bodies in contact.

The first three conditions are expressed in terms of inequalities. The last two conditions represent Coulomb's law of friction.

3. Different Methods for Solution of Contact Problems

The different techniques for solution of contact problems can be divided into three groups: (1) mathematical methods, (2) semiempirical methods, and (3) numerical methods.

3.1. Mathematical Models

Early work on contact problems was concerned with indentation of rigid frictionless bodies into an elastic medium. Most of this work was done in the Soviet Union (Shtaerman, Galin, and Muskhelishvili) and was based on using mathematical methods such as complex potentials, conformal maps, and integral equation methods (refs. 22–25). More recent work is based on the use of variational inequalities (refs. 26 and 27).

3.2. Semiempirical Models

The second group of methods consists of semiempirical approaches, iterative and simple methods based on physical considerations (refs. 28–34). An example of these methods is the gap element approach based on the use of interface elements between the contacting bodies. The stiffnesses of the interface elements are adjusted to allow the relative motion of the two bodies, while preventing penetration of one body into the other. These approaches were found to be sensitive to the selection of the stiffnesses of the interface elements. Improper choice of the stiffnesses can lead to slow convergence, oscillatory behavior, and occasionally divergence. Therefore, they are not recommended for use in tire contact problems.

3.3. Mathematical Programming Approaches

The third group of methods is based on mathematical programming approaches in conjunction

with the finite element method. The two most commonly used methods in this category are the Lagrange multiplier and penalty methods (refs. 19, 35, and 36). In the Lagrange multiplier approach, the contact region is first estimated and the contact conditions, which are treated as equality constraints, are satisfied by transforming the constrained problem into an unconstrained one with the introduction of additional variables (Lagrange multipliers).

Penalty methods, on the other hand, allow the transformation of a constrained problem into an unconstrained one without introducing additional variables. This is accomplished by satisfying the contact conditions only approximately for finite values of the penalty parameter. For frictionless contact, application of the penalty method is equivalent to placing interface springs between all penetrating points and the contact surface.

The Lagrange multiplier and penalty approaches are both computationally expensive (requiring large numbers of elements, degrees of freedom, and iterations) and are sensitive to the manner of updating contact conditions at a contact node. Moreover, the Lagrange multiplier method results in an increase in the number of equations and the presence of zero terms on the main diagonal of the resulting algebraic equations. In the penalty method, the resulting algebraic equations become ill-conditioned for large values of the penalty parameter, and the approximate solutions are sensitive to the choice of the penalty parameter.

Recently, perturbed Lagrangian approaches have been proposed to alleviate the drawbacks of the Lagrange multiplier and penalty methods. The perturbed Lagrangian formulation is obtained from the classical Lagrange multiplier formulation by adding a positive regularization term in the Lagrange multiplier vector (refs. 15, 16, and 19).

4. Key Elements of Proposed Strategy

Figure 1 shows a schematic overview of a proposed computer-aided design (CAD) system for tire design. Such a system is not currently available but would be valuable for the tire designer. An important component of the CAD system is the modeling and analysis module, shown in figure 1. Artificial intelligence (AI) procedures are used in the selection and generation of the mathematical and discrete models. A hierarchy of mathematical models ranging from two-dimensional first-order shear deformation shell theory to a full three-dimensional continuum theory is generated for modeling different regions of the tire. Also, a range of discrete models with different levels of sophistication are generated. These models are used for assessing the quality of the numerical predictions of the tire response and for adaptive improvement of the solutions. The effectiveness of the CAD system depends, to a great extent, on the effectiveness of the computational strategy used in the modeling and analysis module.

5. Proposed Computational Strategy for Tire Contact Problem

The overall goal of the present research is to develop an effective computational strategy for the solution of the tire contact problem which could serve as the modeling and analysis module shown in figure 1. The proposed strategy combines the following characteristics:

1. It enhances the computational efficiency.
2. It provides information about the sensitivity of the tire response to various modeling details.
3. It provides error indicators which identify the regions where more sophisticated continuous mathematical and/or discrete models are needed.
4. It synthesizes the response of the tire, using a complex mathematical (and/or discrete) model, from that of a simpler model (or a sequence of simpler models).

The five key elements of the strategy are (1) semianalytic finite elements, (2) a mixed formulation with the fundamental unknowns consisting of strain parameters, stress-resultant parameters, and generalized displacements, (3) a perturbed Lagrangian procedure for the determination of the contact area and pressure, (4) multilevel operator splitting to effect successive simplifications of the governing equations, and (5) reduction methods and multilevel iterative procedures (through nested applications of the PCG technique).

In the semianalytic finite elements the tire variables and external loadings are represented by Fourier series in the circumferential coordinate and piecewise polynomials in the meridional coordinate. Mixed finite element models are used in which independent polynomial shape functions are used for each of the strain components, stress resultants, and generalized displacements, with the strain components and stress resultants

allowed to be discontinuous at interelement boundaries. The perturbed Lagrangian procedure is based on augmenting the classical Lagrangian functional by a quadratic (positive) term in the Lagrange multiplier vector for regularization. Operator splitting refers to the additive decomposition of the different arrays used in the governing finite element equations. Hierarchical application of operator splitting is used to

1. Uncouple the equations associated with different Fourier harmonics and identify the effects of the different harmonics
2. Delineate contributions to
   a. Symmetric and antisymmetric components of the response with respect to $\theta = 0$
   b. Orthotropic and nonorthotropic (anisotropic) material properties
   c. Simple and more sophisticated models

The aforementioned key elements of the computational strategy are described in the following subsections. The effectiveness of one of the key elements is demonstrated by means of numerical examples in section 6. While each of the key elements contributes to the effectiveness of the computational strategy, the synergism resulting from their combination is expected to have a dramatic effect on the efficiency of the solution process.

5.1. Mathematical Formulation

In the present study the tire is modeled using a moderate-rotation Sanders-Budiansky shell theory with the effects of transverse shear deformation and laminated anisotropic material response included (refs. 37 and 38). A total Lagrangian formulation is used and the fundamental unknowns consist of the five generalized displacements, the eight stress resultants, and the corresponding eight strain components of the middle surface. The sign convention for the different tire stress resultants and generalized displacements is shown in figure 2. The concepts presented in the succeeding sections can be extended to higher order shear deformation theories, as well as to three-dimensional continuum theory

5.1.1. Spatial discretization of the tire. Each of the generalized displacements, the stress resultants, and the strain components is expanded in a Fourier series of the circumferential coordinate θ. The discretization in the meridional direction is performed by using a three-field mixed finite element model. The following expressions are used for approximating the external loading, generalized displacements, stress resultants, and strain components within each element:

$$\begin{Bmatrix} p_s(s,\theta) \\ p_\theta(s,\theta) \\ p(s,\theta) \end{Bmatrix} = \sum_{n=0}^{\infty} N^i \left(\begin{Bmatrix} p^i_{s,n} \\ -p^i_{\theta,n} \\ p^i_n \end{Bmatrix} \cos n\theta + \begin{Bmatrix} \bar{p}^i_{s,n} \\ \bar{p}^i_{\theta,n} \\ \bar{p}^i_n \end{Bmatrix} \sin n\theta \right) \tag{4}$$

$$\begin{Bmatrix} u(s,\theta) \\ v(s,\theta) \\ w(s,\theta) \\ \phi_s(s,\theta) \\ \phi_\theta(s,\theta) \end{Bmatrix} = \sum_{n=0}^{\infty} N^i \left(\begin{Bmatrix} u^i_n \\ -v^i_n \\ w^i_n \\ \phi^i_{s,n} \\ -\phi^i_{\theta,n} \end{Bmatrix} \cos n\theta + \begin{Bmatrix} \bar{u}^i_n \\ \bar{v}^i_n \\ \bar{w}^i_n \\ \bar{\phi}^i_{s,n} \\ \bar{\phi}^i_{\theta,n} \end{Bmatrix} \sin n\theta \right) \tag{5}$$

and

$$\begin{bmatrix} N_s(s,\theta) & \varepsilon_s(s,\theta) \\ N_\theta(s,\theta) & \varepsilon_\theta(s,\theta) \\ N_{s\theta}(s,\theta) & 2\varepsilon_{s\theta}(s,\theta) \\ M_s(s,\theta) & \kappa_s(s,\theta) \\ M_\theta(s,\theta) & \kappa_\theta(s,\theta) \\ M_{s\theta}(s,\theta) & 2\kappa_{s\theta}(s,\theta) \\ Q_s(s,\theta) & 2\varepsilon_{s3}(s,\theta) \\ Q_\theta(s,\theta) & 2\varepsilon_{\theta 3}(s,\theta) \end{bmatrix} = \sum_{n=0}^{\infty} \bar{N}^{i'} \left(\begin{bmatrix} N^{i'}_{s,n} & \varepsilon^{i'}_{s,n} \\ N^{i'}_{\theta,n} & \varepsilon^{i'}_{\theta,n} \\ N^{i'}_{s\theta,n} & 2\varepsilon^{i'}_{s\theta,n} \\ M^{i'}_{s,n} & \kappa^{i'}_{s,n} \\ M^{i'}_{\theta,n} & \kappa^{i'}_{\theta,n} \\ M^{i'}_{s\theta,n} & 2\kappa^{i'}_{s\theta,n} \\ Q^{i'}_{s,n} & 2\varepsilon^{i'}_{s3,n} \\ Q^{i'}_{\theta,n} & 2\varepsilon^{i'}_{\theta 3,n} \end{bmatrix} \cos n\theta + \begin{bmatrix} \bar{N}^{i'}_{s,n} & \bar{\varepsilon}^{i'}_{s,n} \\ \bar{N}^{i'}_{\theta,n} & \bar{\varepsilon}^{i'}_{\theta,n} \\ -\bar{N}^{i'}_{s\theta,n} & -2\bar{\varepsilon}^{i'}_{s\theta,n} \\ \bar{M}^{i'}_{s,n} & \bar{\kappa}^{i'}_{s,n} \\ \bar{M}^{i'}_{\theta,n} & \bar{\kappa}^{i'}_{\theta,n} \\ -\bar{M}^{i'}_{s\theta,n} & -2\bar{\kappa}^{i'}_{s\theta,n} \\ \bar{Q}^{i'}_{s,n} & 2\bar{\varepsilon}^{i'}_{s3,n} \\ -\bar{Q}^{i'}_{\theta,n} & -2\bar{\varepsilon}^{i'}_{\theta 3,n} \end{bmatrix} \sin n\theta \right) \tag{6}$$

where N^i are the polynomial shape functions used in approximating the generalized displacements and external loadings, and $\bar{N}^{i'}$ are the shape functions for the stress resultants and strain components in the meridional direction; the generalized displacements with superscript i and subscript n represent the nodal displacement coefficients associated with the Fourier harmonic n; the stress resultants and strain components with superscript i' and subscript n represent the parameters associated with the Fourier harmonic n. Note that the degree of the shape functions $\bar{N}^{i'}$ is lower than that of N^i. Moreover, the continuity of the stress resultants and strain components is not imposed at the interelement boundaries and, therefore, the stress resultant and strain parameters can be eliminated on the element level.

In equations (4) to (6) the range of the superscript i is the number of displacement nodes in the element; the range of the superscript i' is the number of parameters used in approximating each of the stress resultants and strain components; the shell variables without a bar are the coefficients of the cosine terms, and shell variables with a bar are the coefficients of the sine terms; and a repeated superscript denotes summation over its entire range. Henceforth, the vectors of the 10 generalized displacement parameters (eqs. (5)), of the 16 stress-resultant parameters, and of the 16 strain parameters (eqs. (6)), associated with the harmonic n are denoted by $\{X\}_n$, $\{H\}_n$, and $\{E\}_n$, respectively. These vectors can be decomposed into symmetric and antisymmetric sets (with respect to $\theta = 0$) as shown in table 1.

5.1.2. Governing equations. The governing discrete equations of the tire are obtained by applying a modified form of the three-field Hu-Washizu mixed variational principle. The modification amounts to augmenting the functional of that principle by two terms: the Lagrange multiplier vector associated with the contact forces and a regularization term, which is quadratic in the Lagrange multiplier vector (refs. 15, 16, and 19).

The vector of Lagrange multipliers $\{\lambda\}$, which is used to enforce the contact conditions, is expanded in a Fourier series in the circumferential direction and piecewise polynomials in the meridional direction:

$$\{\lambda\} = \sum_{n=0}^{\infty} \bar{N}^{i'} \left(\{\lambda\}^{i'}_n \cos n\theta + \{\bar{\lambda}\}^{i'}_n \sin n\theta \right) \tag{7}$$

The Lagrange multiplier parameters $\{\lambda\}_n$ are allowed to be discontinuous at interelement boundaries. If the number of terms (harmonics) retained in the Fourier series is $N+1$, the governing equations can be written

in the following compact form:

$$\begin{Bmatrix} f^{(0)} \\ f^{(1)} \\ \vdots \\ f^{(N)} \end{Bmatrix} = \begin{bmatrix} K^{(0)} & & & \\ & K^{(1)} & & \\ & & \ddots & \\ & & & K^{(N)} \end{bmatrix} \begin{Bmatrix} Z_0 \\ Z_1 \\ \vdots \\ Z_N \end{Bmatrix} + \begin{Bmatrix} G^{(0)}(Z_0, Z_1, \ldots, Z_N) \\ G^{(1)}(Z_0, Z_1, \ldots, Z_N) \\ \vdots \\ G^{(N)}(Z_0, Z_1, \ldots, Z_N) \end{Bmatrix} - \begin{Bmatrix} P^{(0)} \\ P^{(1)} \\ \vdots \\ P^{(N)} \end{Bmatrix} = 0 \qquad (8)$$

where $\{Z\}_n$ $(n = 0, 1, ..., N)$ is the vector of unknowns associated with the nth harmonic, which includes strain parameters $\{E\}_n$, stress resultant parameters $\{H\}_n$, generalized displacements $\{X\}_n$, and Lagrange multipliers $\{\lambda\}_n$; $[K]^{(n)}$ are linear matrices, $\{G\}^{(n)}$ are vectors of nonlinear terms, and $\{P\}^{(n)}$ are consistent load vectors. The following observations can be made about the governing equations (eqs. (8)):

1. The first matrix on the left side of equations (8) is block diagonal. This is a direct consequence of the orthogonality of the trigonometric functions, which results in uncoupling the equations associated with the different Fourier harmonics for the linear case. For the nonlinear case, the vectors $\{G\}^{(n)}$ couple the unknowns associated with *all* the harmonics. The different types of coupling that occur in the analysis of tires using semianalytic finite elements are listed in table 2.
2. The contributions of the different Fourier harmonics and the anisotropic (nonorthotropic) material coefficients to the governing equations can be identified as follows:
   a. Fourier harmonics—The block-diagonal matrices $[K]^{(n)}$ $(n > 1)$ in equations (8) are linear in the Fourier harmonic n. Therefore, $[K]^{(n)}$ can be expressed as the sum of two matrices as follows:

$$[K]^{(n)} = [\tilde{K}] + n[\hat{K}] \qquad (9)$$

   where both $[\tilde{K}]$ and $[\hat{K}]$ are independent of n. The nonlinear vectors $\{G\}^{(n)}$ are quadratic in n.
   b. Anisotropy (Nonorthotropy)—A unique feature of the mixed formulation used herein is that the anisotropic (nonorthotropic) material coefficients are included only in the linear matrices $[K]^{(n)}$. For the linear case, these anisotropic coefficients result in the coupling between the symmetric and antisymmetric shell parameters (see table 1).
3. If the vectors $\{Z\}_n$ are partitioned into subvectors of parameters of strains, stress resultants, generalized displacements, and Lagrange multipliers, that is,

$$\{Z\}_n = \begin{Bmatrix} E_n \\ H_n \\ X_n \\ \lambda_n \end{Bmatrix} \qquad (10)$$

   then the matrix $[K]^{(n)}$ can be written in the following form:

$$[K]^{(n)} = \begin{bmatrix} K_o + K_a & -R & \cdot & \cdot \\ -R^t & \cdot & S_o^t + nS & \cdot \\ \cdot & S_o^t + nS^t & \cdot & Q \\ \cdot & \cdot & Q^t & R/\varepsilon \end{bmatrix} \qquad (11)$$

   where the submatrices $[K_o]$ and $[K_a]$ contain the contributions of the orthotropic and anisotropic (nonorthotropic) material coefficients, and ε is a penalty parameter. The explicit forms of the matrices $[K_o]$, $[K_a]$, $[S_o]$, $[S]$, and $[R]$ are given in references 14 and 39.
4. The nonlinear vectors $\{G\}^{(n)}$ contain bilinear terms in $\{H\}_n$ and $\{X\}_n$, as well as quadratic terms in $\{X\}_n$.

5.2. Generation of the Nonlinear Response of the Tire

For a given external loading, the governing nonlinear equations (eqs. (8)) are solved by using the Newton-Raphson iterative technique. The recursion formulas for the rth iterational cycle are

$$\left(\begin{bmatrix} K^{(0)} & & & \\ & K^{(1)} & & \\ & & \ddots & \\ & & & K^{(N)} \end{bmatrix} + \begin{bmatrix} \bar{K}^{(00)} & \bar{K}^{(01)} & \dots & \bar{K}^{(0N)} \\ & 0 & \dots & \bar{K}^{(1N)} \\ & & \ddots & \vdots \\ & & & 0 \end{bmatrix}\right)^{(r)} \begin{Bmatrix} \Delta Z_0 \\ \Delta Z_1 \\ \vdots \\ \Delta Z_N \end{Bmatrix}^{(r)} = - \begin{Bmatrix} f^{(0)} \\ f^{(1)} \\ \vdots \\ f^{(N)} \end{Bmatrix}^{(r)} \tag{12}$$

and

$$\begin{Bmatrix} Z_0 \\ Z_1 \\ \vdots \\ Z_N \end{Bmatrix}^{(r+1)} = \begin{Bmatrix} Z_0 \\ Z_1 \\ \vdots \\ Z_N \end{Bmatrix}^{(r)} + \begin{Bmatrix} \Delta Z_0 \\ \Delta Z_1 \\ \vdots \\ \Delta Z_N \end{Bmatrix}^{(r)} \tag{13}$$

where

$$[\bar{K}]^{(IJ)} = \frac{\partial}{\partial Z_J}[G]^{(I)} \qquad (I, J = 1 \text{ to } N) \tag{14}$$

For each Newton-Raphson iteration (represented by eqs. (12) and (13)), two nested iteration loops are performed using the preconditioned conjugate gradient (PCG) technique as follows:

1. The inner iteration loop accounts for the coupling between the different harmonics, that is, the submatrices $[\bar{K}]^{(IJ)}$.
2. The outer loop accounts for the contact conditions (the matrices $[Q]$ and $[R]$ associated with the contact nodes, eqs.(11)).

In the inner loop the following uncoupled equations are solved:

$$\left.\begin{aligned} ([K]^{(0)} + [\bar{K}]^{(00)(r)})\{\Delta Z\}_0^{(r)} = & - \{f\}^{(0)(r)} - \check{\lambda}([\bar{K}]^{(01)}\{\Delta Z\}_1 \\ & + [\bar{K}]^{(02)}\{\Delta Z_2\} + \cdots + [\bar{K}]^{(0N)}\{\Delta Z_N\})^{(r)} \\ [K]^{(1)}\{\Delta Z\}_1^{(r)} = & - \{f\}^{(1)(r)} - \check{\lambda}([\bar{K}]^{(10)}\{\Delta Z\}_0 + [\bar{K}]^{(12)}\{\Delta Z\}_2 \\ & + \cdots + [\bar{K}]^{(1N)}\{\Delta Z\}_N)^{(r)} \\ & \vdots \\ [K]^{(N)}\{\Delta Z\}_N^{(r)} = & - \{f\}^{(N)(r)} - \check{\lambda}([\bar{K}]^{(N0)}\{\Delta Z\}_0 \\ & + [\bar{K}]^{(N1)}\{\Delta Z\}_1 + \cdots)^{(r)} \end{aligned}\right\} \tag{15}$$

where $\check{\lambda}$ is a tracing parameter which identifies the coupling between the different Fourier harmonics. Note that because of the special structure of the Jacobian matrix in equations (12), only the left side associated with the zeroth harmonic needs to be updated in each iteration.

An efficient technique is described in the next subsection for solving equations (15). The major advantage of nested application of PCG is the reduction in the total number of iterations required for convergence.

5.3. Efficient Generation of the Response Associated With Different Harmonics

An efficient procedure is presented herein for generating the tire responses associated with different harmonics (solution of eqs. (15)). The basic idea of this procedure is to approximate the tire response associated

with the range of Fourier harmonics, $1 \leq n \leq N$, by a linear combination of a few global approximation vectors that are generated at a particular value of the Fourier harmonic within that range. The full equations of the finite element model are solved for only a single Fourier harmonic, and the responses corresponding to the other Fourier harmonics are generated using a reduced system of equations with considerably fewer degrees of freedom. The proposed procedure can be conveniently divided into two phases: (1) restructuring equations (15), for $1 \leq n \leq N$, to delineate the dependence on the Fourier harmonic n, and (2) generation of global approximation vectors (or modes) to approximate the response associated with a range of values of the Fourier harmonic and determination of the amplitudes of the modes. The procedure is described subsequently.

5.3.1. Restructuring of the governing equations. If equations (9) and (11) are used, the governing equations for the harmonic n ($1 \leq n \leq N$) can be embedded in a single-parameter family of equations and written in the following compact form:

$$([\tilde{K}] + n[\hat{K}])\{\Delta Z\}_n = \{P(n)\} + \check{\lambda}\{\hat{P}(n)\} \tag{16}$$

The two vectors $\{P(n)\}$ and $\{\hat{P}(n)\}$ are quadratic in n.

5.3.2. Basis reduction and reduced system of equations. The basis reduction is achieved by approximating the vectors $\{\Delta Z\}_n$, for a certain range of Fourier harmonics, $1 \leq n \leq N$, by a linear combination of a few global approximation vectors which are generated at a particular value of the Fourier harmonic within that range. The approximation is expressed by the following transformation:

$$\{\Delta Z\}_n = [\Gamma]\{\psi\}_n \tag{17}$$

where $[\Gamma]$ is a transformation matrix whose columns are the preselected approximation vectors, and $\{\psi\}_n$ is a vector of unknown parameters representing the amplitudes of the global approximation vectors for the harmonics n. The number of components of $\{\psi\}_n$ is much less than the number of components of $\{\Delta Z\}_n$.

A Bubnov-Galerkin technique is now used to replace the original equations (eqs. (16)) by the following reduced equations in $\{\psi\}_n$:

$$\left([\tilde{k}] + n[\hat{k}]\right)\{\psi\}_n = \{q\} + \check{\lambda}\{\hat{q}\} \tag{18}$$

where

$$[\tilde{k}] = [\Gamma]^t[\tilde{K}][\Gamma] \tag{19}$$

$$[\hat{k}] = [\Gamma]^t[\hat{K}][\Gamma] \tag{20}$$

$$\{q\} = [\Gamma]^t\{P(n)\} \tag{21}$$

$$\{\hat{q}\} = [\Gamma]^t\{\hat{P}(n)\} \tag{22}$$

5.3.3. Selection and generation of global approximation vectors. The global approximation vectors are selected to be the response associated with a single Fourier harmonic n_o and its various-order derivatives with respect to n. Henceforth, the derivatives of the response with respect to n are referred to as "path derivatives." The matrix $[\Gamma]$ in equations (17) is therefore given by

$$[\Gamma] = [\{\Delta z\} \quad \frac{\partial}{\partial n}\{\Delta Z\} \quad \frac{\partial^2}{\partial n^2}\{\Delta Z\}\ldots]_{n_o} \tag{23}$$

The path derivatives are obtained by successive differentiation of the governing equations (eqs. (16)). The recursion relations for the first three global approximation vectors can be written in the following form:

$$([\tilde{K}] + n_o[\hat{K}])\{\Delta Z\}_{n_o} = \frac{\partial}{\partial n}\{P\} + \check{\lambda}\frac{\partial}{\partial n}\{\hat{P}\} \tag{24}$$

$$([\tilde{K}] + n_o[\hat{K}])\frac{\partial}{\partial n}\{\Delta Z\}_{n_o} = \frac{\partial^2}{\partial n^2}\{P\} + \check{\lambda}\frac{\partial^2}{\partial n^2}\{\hat{P}\} - [\hat{K}]\{\Delta Z\}_{n_o} \tag{25}$$

$$([\tilde{K}] + n_o[\hat{K}])\frac{\partial^2}{\partial n^2}\{\Delta Z\}_{n_o} = \frac{\partial^3}{\partial n^3}\{P\} + \check{\lambda}\frac{\partial^3}{\partial n^3}\{\hat{P}\} - 2[\hat{K}]\frac{\partial}{\partial n}\{\Delta Z\}_{n_o} \tag{26}$$

Note that the left-side matrix in equations (24) to (26) is the same, and therefore, it needs to be decomposed only once in the process of generating all the global approximation vectors.

5.3.4. Comments on proposed procedure. The following comments are made concerning the foregoing procedure for generating the responses associated with different harmonics:

1. The particular choice of the global approximation vectors used herein provides a direct quantitative measure of the sensitivity of the different response quantities of the tire to the circumferential wave number (the Fourier harmonic) n.
2. For problems requiring large numbers of Fourier harmonics (e.g., 100 or more), the range of n is divided into intervals of fewer (e.g., 10) harmonics each; the global approximation vectors and reduced equations are generated at an intermediate value of n within each interval, and the responses associated with the values of n within that interval are generated by the foregoing procedure. Note that higher accuracy of the reduced solutions can be obtained by marching backward as well as forward in the n-space with the reduced equations.
3. The computational effort can be further reduced by using the procedure outlined in reference 16 to uncouple the equations associated with the symmetric and antisymmetric shell parameters (with respect to $\theta = 0$). The procedure is based on transferring the anisotropic (nonorthotropic) terms (submatrices $[K_a]$ in eqs. (11)) to the right sides of equations (15), and adding another level of PCG iterations to account for them.

6. Numerical Studies

To evaluate the effectiveness of the procedure described in the preceding section for generating the response associated with different harmonics, a number of problems have been solved by this procedure. For each problem, the solution obtained by the foregoing procedure was compared with the direct solution of all the equations associated with the different harmonics. Herein, the solutions are presented for a linear problem of a two-layered anisotropic tire with elliptic cross section. The material and geometric characteristics of the tire are shown in figure 3. The loading consists of uniform inflation pressure and a localized normal loading simulating contact pressure. The normal loading in pascals is given by the following equations, which model experimental data obtained at NASA Langley:

$$p = \begin{cases} 6.895 \times 10^5 - \frac{p_o\beta}{\pi} - \sum_{n=1}^{10} p_n \cos n\theta & (-0.2 < \xi < 0.2) \\ 6.895 \times 10^5 & (|\ \xi\ | > 0.2) \end{cases} \tag{27}$$

where

$$p_n = \frac{2p_o}{n\pi}\sin n\beta \tag{28}$$

and p_o and β are functions of ξ as shown in figure 4.

Three-field mixed finite element models were used for the discretization in the meridional direction. Because of the symmetry of the shell meridian and loading, only one-half of the meridian is analyzed using 20 elements. The boundary conditions at the centerline are taken to be the symmetric or antisymmetric conditions. Quadratic Lagrangian interpolation functions are used for approximating each of the stress resultants and strain components, and cubic Lagrangian interpolation functions are used for approximating each of the generalized displacements (a total of 960 stress-resultant parameters, 960 strain parameters, and 603 nonzero displacement degrees of freedom). The integrals in the governing equations are evaluated using a three-point Gauss-Legendre numerical quadrature formula. Typical results are presented in figures 5 to 10 and in tables 3 and 4.

The foregoing procedure was applied to this problem, and 10 global approximation vectors were evaluated at $n_o = 5$ and used to generate the tire response in the range $n = 1$ to 10. The accuracy of the generalized displacements and total strain energy obtained by the foregoing strategy with 5, 8, and 10 global approximation

vectors is indicated in figures 5, 6, and 7. Each generalized displacement in figures 5 and 6 is normalized by dividing by its maximum absolute value given in tables 3 and 4. The generalized displacements and total strain energy predicted by the foregoing procedure with 10 vectors are almost indistinguishable from the direct finite element solution.

To contrast the accuracy of the predictions of the foregoing procedure with that of the Taylor series expansions, the solutions obtained using 8 and 10 terms of the Taylor series expansion at $n_o = 5$ are shown in figures 8 and 9. As can be seen, the predictions of the Taylor series are considerably less accurate than the predictions of the foregoing strategy, particularly when n is much different from n_o (the series diverges when $n > 9$). Normalized contour plots for the total generalized displacements produced by the combined inflation pressure and localized loading are shown in figure 10.

7. Experimental Verification of Tire Contact and Deformation

One of the most important aspects of tire modeling is verification of the numerically predicted tire deformations and stresses. To aid in the verification process, a sizable experimental program is underway to measure the responses of various tires subjected to different loading conditions. The Space Shuttle orbiter nose gear tire has been selected as one of the aircraft tires to be analyzed. The measured responses of this tire are being included in the experimental data base.

Figure 11 shows the measured pressure distribution and friction coefficient distribution for a Space Shuttle orbiter nose gear tire inflated to 2.17 MPa and subjected to a static load of 67 kN. The loading conditions shown in the figure are typical operating loads for the orbiter nose gear tire. The load-deflection curve for the tire inflated to 2.17 MPa is shown in figure 12. The data presented in the figure provide a global measurement of structural response of the orbiter tire to the static loading condition.

To obtain a detailed map of the tire deformations under static loading conditions, close-range photogrammetry techniques are being utilized. Figure 13 is a photograph of the experimental arrangement used to obtain these photogrammetry measurements. A video camera is used to measure accurately the spatial coordinates of each of the circular targets bonded to the tire sidewall. By using target-location data from various loading conditions, a map of tire deformations can be constructed. Figure 14 shows a three-dimensional representation of sidewall deformations of the orbiter nose gear tire subjected to an inflation pressure of 2.17 MPa and loaded statically to 58 kN.

8. Benchmark Problems

The National Tire Modeling Program (NTMP), which is jointly sponsored by the National Aeronautics and Space Administration and the U.S. tire industry, has defined a family of benchmark tire modeling problems. The initial set of benchmark problems includes four loading conditions of increasing complexity. The loading conditions are represented schematically in figure 15. The first loading condition is axisymmetric and each of the subsequent three loading conditions reduces the degree of symmetry. Specifically, the four loading conditions are (1) inflation pressure only, (2) combined inflation pressure and static vertical loading on a flat surface, (3) combined inflation pressure, static vertical loading on a flat surface, and an externally applied drag load, and (4) combined inflation pressure, static vertical loading on a flat surface, and an externally applied lateral force.

A number of passenger car, truck, and aircraft tires will be subjected to the aforementioned loading conditions. These tires will be representative of the different construction techniques currently in use, that is, bias-ply, bias-belted, and radial-belted designs. The various tire manufacturers participating in the NTMP will furnish the test tires for the benchmark experimental program. The manufacturers are also furnishing samples of the rubber, cord, and ply stock materials so that detailed studies of the material properties of the tire constituents can be conducted.

9. Future Directions of Research

Although considerable effort has recently been devoted to the development of analytical tire design tools, major advances are still needed in computational strategies and numerical algorithms, including contact algorithms, in order that these analytical tools play an important role in tire design. For advancement to be made, a number of pacing items must be addressed by the research community. Primary pacing items recommended as future directions for research include (1) development of computational models for flexible cord-rubber materials, (2) accurate determination of the operational loads on tires, and (3) assessment of the reliability of numerical response predictions and their adaptive improvement. The secondary pacing items include

(1) development of automatic model generation facilities and (2) integration of tire analysis programs into CAD systems.

9.1. Primary Pacing Items

9.1.1. Computational models for flexible cord-rubber materials. The reliability of numerical predictions of tire response is critically dependent on accurate constitutive modeling of the material behavior in the entire range of operational loads and temperatures. Also, numerical techniques are needed for predicting the failure initiation and damage propagation in tires. This, in turn, may require the availability of microstructurally based constitutive descriptions and damage theories.

9.1.2. Accurate determination of the operational loads on tires. The service loads on tires that are difficult to determine include impact forces, thermal loads, and contact forces and, in turn, determination of these forces requires accurate determination of braking, skidding, and frictional forces. The modeling of frictional forces needs special attention, specifically related to the effect of inflation pressure. Moreover, because of the uncertainties associated with external forces, as well as the material and geometric properties of the tire, there is a need to quantify the uncertainty in the response predictions of the tire through the use of stochastic models and probabilistic analysis techniques. A state-of-the-art review of probabilistic methods for engineering analysis is given in reference 40.

9.1.3. Assessment of reliability and adaptive improvement of numerical response predictions. In spite of the considerable attention devoted by engineers and mathematicians to the subject of error estimation and control, none of the large-scale commercial finite element systems has facilities for error estimation or adaptive improvement. To remedy this situation, major advances are needed in the theory, strategies, and algorithms for implementation of error estimation and control.

Maturation of the technology of estimation and control of discretization errors and incorporation of this technology into general-purpose tire analysis and design systems will allow the tire designer to select only the initial discrete model which is sufficient to approximate the geometry of the tire, the error measure, and the tolerance. Then the analysis system can automatically refine the model until the selected error measure falls below the prescribed tolerance. The strategy for adaptive improvement can either be specified by the user or automatically selected by the program (possibly with the aid of an AI-based expert system) in such a manner as to minimize the cost of the analysis.

9.2. Secondary Pacing Items

9.2.1. Development of automatic model generation facilities. One of the most important steps for the accurate prediction of the response of a tire is the proper selection of the mathematical and discrete models. Hence, the development of automatic model generation facilities as well as knowledge-based and expert systems is needed to help the tire analyst and designer in the initial selection of the model, its adaptive refinement, and the interpretation of results. An example of the recent work on automatic model generation is given in reference 41.

9.2.2. Integration of tire analysis programs into CAD systems. Much effort is now being directed to the integration of analysis programs into CAD systems. With the trend of moving from software-based processing to hardware-based processing, some of the analysis modules for the tire are likely to become hardware functions. The interface between, and optimal combination of, software and hardware functions should be investigated.

10. Summary and Conclusions

Currently used techniques for tire contact analysis are reviewed. Discussion focuses on the techniques used in modeling frictional forces and the treatment of contact conditions. A status report is presented on a new computational strategy for the modeling and analysis of tires including the solution of the contact problem. The strategy is based on solution of the complex tire contact problem, as a sequence of simpler problems, and obtaining information about the sensitivity of the tire response to each of the complicating factors.

The key elements of the proposed strategy are (1) semianalytic finite elements in which the shell variables are represented by Fourier series in the circumferential direction and piecewise polynomials in the meridional direction, (2) a mixed formulation with the fundamental unknowns consisting of strain parameters, stress-resultant parameters, and generalized displacements, (3) a perturbed Lagrangian formulation for the determination of the contact area and pressure, (4) multilevel operator splitting to effect successive simplifications of the governing equations, and (5) multilevel iterative procedures and reduction techniques to generate the response of the tire.

The governing discrete equations of the tire are obtained by applying a modified form of the three-field Hu-Washizu mixed variational principle. The

modification consists of augmenting the functional of that principle by two terms: the Lagrange multiplier vector associated with the nodal contact forces and a regularization term (which is quadratic in the Lagrange multiplier vector). Multilevel operator splitting is used to (1) uncouple the equations associated with different harmonics, (2) identify the effects of different Fourier harmonics, and (3) delineate the effect of anisotropic (nonorthotropic) material properties.

The nonlinear governing finite element equations of the tire contact problem are solved using the Newton-Raphson iterative procedure. For each Newton-Raphson iteration, nested iteration loops are performed using the preconditioned conjugate gradient (PCG) technique. The inner iteration loop accounts for the coupling between the different harmonics, and the outer loop accounts for the contact conditions associated with the contact nodes.

An efficient procedure is presented for the solution of the resulting algebraic equations of the inner iteration loop, associated with different Fourier harmonics. The procedure is based on approximating the tire response associated with a range of Fourier harmonics by a few global approximation vectors that are generated at a particular value of the Fourier harmonic within that range. The full equations of the finite element model are thus solved for only a single Fourier harmonic, and the responses corresponding to the Fourier harmonics are generated using a reduced system with considerably fewer degrees of freedom. The effectiveness of this procedure is demonstrated by means of a numerical example of the linear response of a two-layered anisotropic tire subjected to combined inflation pressure and localized loading (simulating the contact pressure).

Experimental research currently underway to verify the numerical predictions of the tire response is discussed, and the benchmark problems selected by the National Tire Modeling Program are described. Also, future directions for research on tire modeling and analysis are recommended.

Results of the present study suggest the following conclusions relative to the proposed computational procedure for generating the tire response associated with different Fourier harmonics:

1. The use of path derivatives (derivatives of the response with respect to the Fourier harmonic) as global approximation vectors leads to accurate solutions with a small number of vectors. Therefore, the time required to solve the reduced equations is relatively small and the total time required to generate the response for a range of 10 Fourier harmonics is little more than that required for a *single* Fourier harmonic.
2. The global approximation vectors provide a direct measure of the sensitivity of the different response quantities to the circumferential wave number (wave harmonic). The sensitivity of the global response can also be assessed with these vectors.
3. The reduction method used in the proposed computational procedure exploits the best elements of the finite element method and of the Bubnov-Galerkin technique, as follows:
   a. The finite element method is used as a general approach for generating global approximation vectors. The full finite element equations are solved only for a single Fourier harmonic.
   b. The Bubnov-Galerkin technique is used as an efficient procedure for minimizing and distributing the error throughout the structure.
4. The reduction method extends the range of applicability of the Taylor series expansion by relaxing the requirement of using small changes in the circumferential wave number.

NASA Langley Research Center
Hampton, Virginia 23665-5225
December 23, 1987

References

1. Tanner, John A.; Stubbs, Sandy M.; and McCarty, John L.: *Static and Yawed-Rolling Mechanical Properties of Two Type VII Aircraft Tires.* NASA TP-1863, 1981.
2. Stubbs, Sandy M.; Tanner, John A.; and Smith, Eunice G.: *Behavior of Aircraft Antiskid Braking Systems on Dry and Wet Runway Surfaces—A Slip-Velocity-Controlled, Pressure-Bias-Modulated System.* NASA TP-1051, 1979.
3. Tanner, John A.; Dreher, Robert C.; Stubbs, Sandy M.; and Smith, Eunice G.: *Tire Tread Temperatures During Antiskid Braking and Cornering on a Dry Runway.* NASA TP-2009, 1982.
4. Oden, J. T.; and Martins, J. A. C.: Models and Computational Methods for Dynamic Friction Phenomena. *Comput. Methods Appl. Mech. & Eng.*, vol. 52, no. 1–3, Sept. 1985, pp. 527–634.
5. Clark, Samuel K.; and Dodge, Richard N.: *Heat Generation in Aircraft Tires Under Free Rolling Conditions.* NASA CR-3629, 1982.
6. Clark, Samuel K.; and Dodge, Richard N.: *Heat Generation in Aircraft Tires Under Braked Rolling Conditions.* NASA CR-3768, 1984.
7. McCarty, John Locke; and Tanner, John A.: *Temperature Distribution in an Aircraft Tire at Low Ground Speeds.* NASA TP-2195, 1983.
8. Schaeffer, Harry G.; and Ball, Robert E.: Nonlinear Deflections of Asymmetrically Loaded Shells of Revolution. AIAA Paper No. 68-292, Apr. 1968.

9. Wunderlich, W.; Cramer, H.; and Obrecht, H.: Application of Ring Elements in the Nonlinear Analysis of Shells of Revolution Under Nonaxisymmetric Loading. *Comput. Methods Appl. Mech. & Eng.*, vol. 51, no. 1–3, Sept. 1985, pp. 259–275.
10. Noor, Ahmed K.: On Making Large Nonlinear Problems Small. *Comput. Methods Appl. Mech. & Eng.*, vol. 34, no. 1–3, Sept. 1982, pp. 955–985.
11. Noor, Ahmed K.; Andersen, Carl M.; and Tanner, John A.: *Mixed Models and Reduction Techniques for Large-Rotation, Nonlinear Analysis of Shells of Revolution With Application to Tires.* NASA TP-2343, 1984.
12. Noor, Ahmed K.: Reduction Method for the Non-Linear Analysis of Symmetric Anisotropic Panels. *Int. J. Numer. Methods Eng.*, vol. 23, 1986, pp. 1329–1341.
13. Noor, Ahmed K.; and Peters, Jeanne M.: Nonlinear Analysis of Anisotropic Panels. *AIAA J.*, vol. 24, no. 9, Sept. 1986, pp. 1545–1553.
14. Noor, Ahmed K.; Andersen, Carl M.; and Tanner, John A.: *Exploiting Symmetries in the Modeling and Analysis of Tires.* NASA TP-2649, 1987.
15. Simo, Juan C.; Wriggers, Peter; and Taylor, Robert L.: A Perturbed Lagrangian Formulation for the Finite Element Solution of Contact Problems. *Comput. Methods Appl. Mech. & Eng.*, vol. 50, no. 2, Aug. 1985, pp. 163–180.
16. Stein, E.; Wagner, W.; and Wriggers, P.: Finite Element Postbuckling Analysis of Shells With Nonlinear Contact Constraints. *Finite Element Methods for Nonlinear Problems*, P. G. Bergan, K. J. Bathe, and W. Wunderlich, eds., Springer-Verlag, c.1986, pp. 719–744.
17. Concus, Paul; Golub, Gene H.; and O'Leary, Dianne P.: A Generalized Conjugate Gradient Method for the Numerical Solution of Elliptic Partial Differential Equations. *Sparse Matrix Computations*, James R. Bunch and Donald J. Rose, eds., Academic Press Inc., 1976, pp. 309–332.
18. Adams, Loyce: m-Step Preconditioned Conjugate Gradient Methods. *SIAM J. Sci. & Stat. Comput.*, vol. 6, no. 2, Apr. 1985, pp. 452–463.
19. Wriggers, Peter; and Nour-Omid, Bahram: *Solution Methods for Contact Problems.* Rep. No. UCB/SESM-84/09 (Contract N00014-76-C-0013), Dep. of Civil Engineering, Univ. of California, July 1984.
20. Tabor, David: Friction—The Present State of Our Understanding. *J. Lubr. Technol.*, vol. 103, no. 2, Apr. 1981, pp. 169–179.
21. Oden, J. T.; and Pires, E. B.: Nonlocal and Nonlinear Friction Laws and Variational Principles for Contact Problems in Elasticity. *J. Appl. Mech.*, vol. 50, no. 1, Mar. 1983, pp. 67–76.
22. Shtaerman, Ilia Iakovlevich: *Kontaktnaya Zadacha Teorii Uprugosti.* Gosudarstvenoe Izdatel'stvo Tekhniko-Teoreticheskoi Literatury (Moscow), 1949.
23. Galin, L. A.: *Contact Problems of Elasticity.* Izdatel'stvo Nauka (Moscow), 1980.
24. Muskhelishvili, N. I. (J. R. M. Radok, transl.): *Some Basic Problems of the Mathematical Theory of Elasticity,* Fourth ed. P. Noordhoff, Ltd. (Groningen), 1963.
25. Glowinski, Roland; Lions, Jacques-Louis; and Trémolières, Raymond: *Numerical Analysis of Variational Inequalities.* North-Holland Publ. Co., 1981.
26. Fredriksson, B.; Rydholm, G.; and Sjöblom, P.: Variational Inequalities in Structural Mechanics With Emphasis on Contact Problems. *Finite Elements in Nonlinear Mechanics, Volume 2,* Pål G. Bergan, Per Kr. Larsen, Hans Pettersson, Alf Samuelsson, Tore Soreide, and Nils-Erik Wiberg, eds., Tapir Publ. (Norway), c.1978, pp. 863–884.
27. Gladwell, G. M. L.: *Contact Problems in the Classical Theory of Elasticity.* Sijthoff & Noordhoff (Netherlands), 1980.
28. Chan, S. K.; and Tuba, I. S.: A Finite Element Method for Contact Problems of Solid Bodies—Part I. Theory and Validation. *Int. J. Mech. Sci.*, vol. 13, no. 7, July 1971, pp. 615–625.
29. Francavilla, A.; and Zienkiewicz, O. C.: A Note on Numerical Computation of Elastic Contact Problems. *Int. J. Numer. Methods Eng.*, vol. 9, no. 4, 1975, pp. 913–924.
30. Hughes, Thomas J. R.; Taylor, Robert L.; Sackman, Jerome L.; Curnier, Alain; and Kanoknukulchai, Worsak: A Finite Element Method for a Class of Contact-Impact Problems. *Comput. Methods Appl. Mech. & Eng.*, vol. 8, no. 3, July–Aug. 1976, pp. 249–276.
31. Okamoto, Noriaki; and Nakazawa, Masaru: Finite Element Incremental Contact Analysis With Various Frictional Conditions. *Int. J. Numer. Methods Eng.*, vol. 14, no. 3, 1979, pp. 337–357.
32. Stadter, J. T.; and Weiss, R. O.: Analysis of Contact Through Finite Element Gaps. *Comput. & Struct.*, vol. 10, no. 6, Dec. 1979, pp. 867–873.
33. Tielking, J. T.; and Schapery, R. A.: A Method for Shell Contact Analysis. *Comput. Methods Appl. Mech. & Eng.*, vol. 26, no. 2, May 1981, pp. 181–195.
34. Ridha, R. A.; Satyamurthy, K.; and Hirschfelt, L. R.: Finite Element Modeling of a Homogeneous Pneumatic Tire Subjected to Footprint Loadings. *Tire Sci. & Technol.*, vol. 13, no. 2, Apr.–June 1985, pp. 91–110.
35. Kikuchi, N.; and Oden, J. T.: *Contact Problems in Elasticity—A Study of Variational Inequalities and Finite Element Methods.* SIAM, 1988.
36. Kikuchi, Noboru, and Song, Young Joon: Penalty/Finite-Element Approximations of a Class of Unilateral Problems in Linear Elasticity. *Q. Appl. Math.*, vol. 39, no. 1, Apr. 1981, pp. 1–22.
37. Sanders, J. Lyell, Jr.: Nonlinear Theories for Thin Shells. *Q. Appl. Math.*, vol. XXI, no. 1, Apr. 1963, pp. 21–36.
38. Budiansky, Bernard: Notes on Nonlinear Shell Theory. *Trans. ASME, Ser. E: J. Appl. Mech.*, vol. 35, no. 2, June 1968, pp. 393–401.
39. Noor, Ahmed K.; and Peters, Jeanne M.: Vibration Analysis of Laminated Anisotropic Shells of Revolution. *Comput. Methods Appl. Mech. & Eng.*, vol. 61, no. 3, Apr. 1987, pp. 277–301.
40. Cruse, T. A.: Probabilistic Structural Analysis Methods (PSAM) for Select Space Propulsion System Structural Components. *Structural Integrity and Durability*

of Reusable Space Propulsion Systems, NASA CP-2471, 1987, pp. 121–125.

41. Shephard, Mark S.: Finite Element Modeling Within an Integrated Geometric Modeling Environment. *Eng. Comput.*, vol. 1, no. 2, 1985:
    Part I—Mesh Generation, pp. 61–71.
    Part II—Attribute Specification, pp. 73–85.

Table 1. Symmetric and Antisymmetric Tire Parameters With Respect to $\theta = 0$

	Symmetric Set	Antisymmetric Set
	Strain components	
$\{E\}_n$	$\varepsilon_{s,n}$, $\varepsilon_{\theta,n}$, $2\bar{\varepsilon}_{s\theta,n}$, $\kappa_{s,n}$, $\kappa_{\theta,n}$, $2\bar{\kappa}_{s\theta,n}$, $2\varepsilon_{s3,n}$, $2\bar{\varepsilon}_{\theta 3,n}$	$\bar{\varepsilon}_{s,n}$, $\bar{\varepsilon}_{\theta,n}$, $2\varepsilon_{s\theta,n}$, $\bar{\kappa}_{s,n}$, $\bar{\kappa}_{\theta,n}$, $2\kappa_{s\theta,n}$, $2\bar{\varepsilon}_{s3,n}$, $2\varepsilon_{\theta 3,n}$
	Stress resultants	
$\{H\}_n$	$N_{s,n}$, $N_{\theta,n}$, $\bar{N}_{s\theta,n}$, $M_{s,n}$, $M_{\theta,n}$, $\bar{M}_{s\theta,n}$, $Q_{s,n}$, $\bar{Q}_{\theta,n}$	$\bar{N}_{s,n}$, $\bar{N}_{\theta,n}$, $N_{s\theta,n}$, $\bar{M}_{s,n}$, $\bar{M}_{\theta,n}$, $M_{s\theta,n}$, $\bar{Q}_{s,n}$, $Q_{\theta,n}$
	Generalized displacements	
$\{X\}_n$	u_n, $\bar{v}_n$, w_n, $\phi_{s,n}$, $\bar{\phi}_{\theta,n}$	$\bar{u}_n$, v_n, $\bar{w}_n$, $\bar{\phi}_{s,n}$, $\phi_{\theta,n}$

Table 2. Different Types of Coupling in the Analysis of Tires Using Semianalytic Finite Elements

Response	Material	Governing finite element equations
Linear	Isotropic or orthotropic	Uncoupled in harmonics Symmetric and antisymmetric variables uncoupled
	Anisotropic	Uncoupled in harmonics Symmetric and antisymmetric variables uncoupled
Nonlinear	Anisotropic	Coupled in harmonics Symmetric and antisymmetric variables coupled

Table 3. Maximum Absolute Values of the In-Plane Displacements and Rotation Components for Two-Layered Anisotropic Tire

[Tire shown in fig. 3; $p_{o\max} = 3.0 \times 10^5$ Pa]

Displacements and rotations	Fourier harmonic		
	$n = 1$	$n = 5$	$n = 10$
$u_n E_T/(p_{o\max} h)$	7.801	0.2570	0.06650
$v_n E_T/(p_{o\max} h)$	.5052	.04869	.02283
$\phi_{s,n} E_T/p_{o\max}$	3.176	.2229	.09105
$\phi_{\theta,n} E_T/p_{o\max}$	.2518	.05846	.3421

Table 4. Maximum Absolute Values of the Normal Displacement Components w_n for Two-Layered Anisotropic Tire

[Tire shown in fig. 3; $p_{o\max} = 3.0 \times 10^5$ Pa]

Fourier harmonic, n	$w_n E_T/(p_{o\max} h)$	Fourier harmonic, n	$w_n E_T/(p_{o\max} h)$
1	13.24	6	0.6496
2	7.047	7	.2262
3	3.667	8	.5758
4	2.253	9	.7861
5	1.351	10	.7717

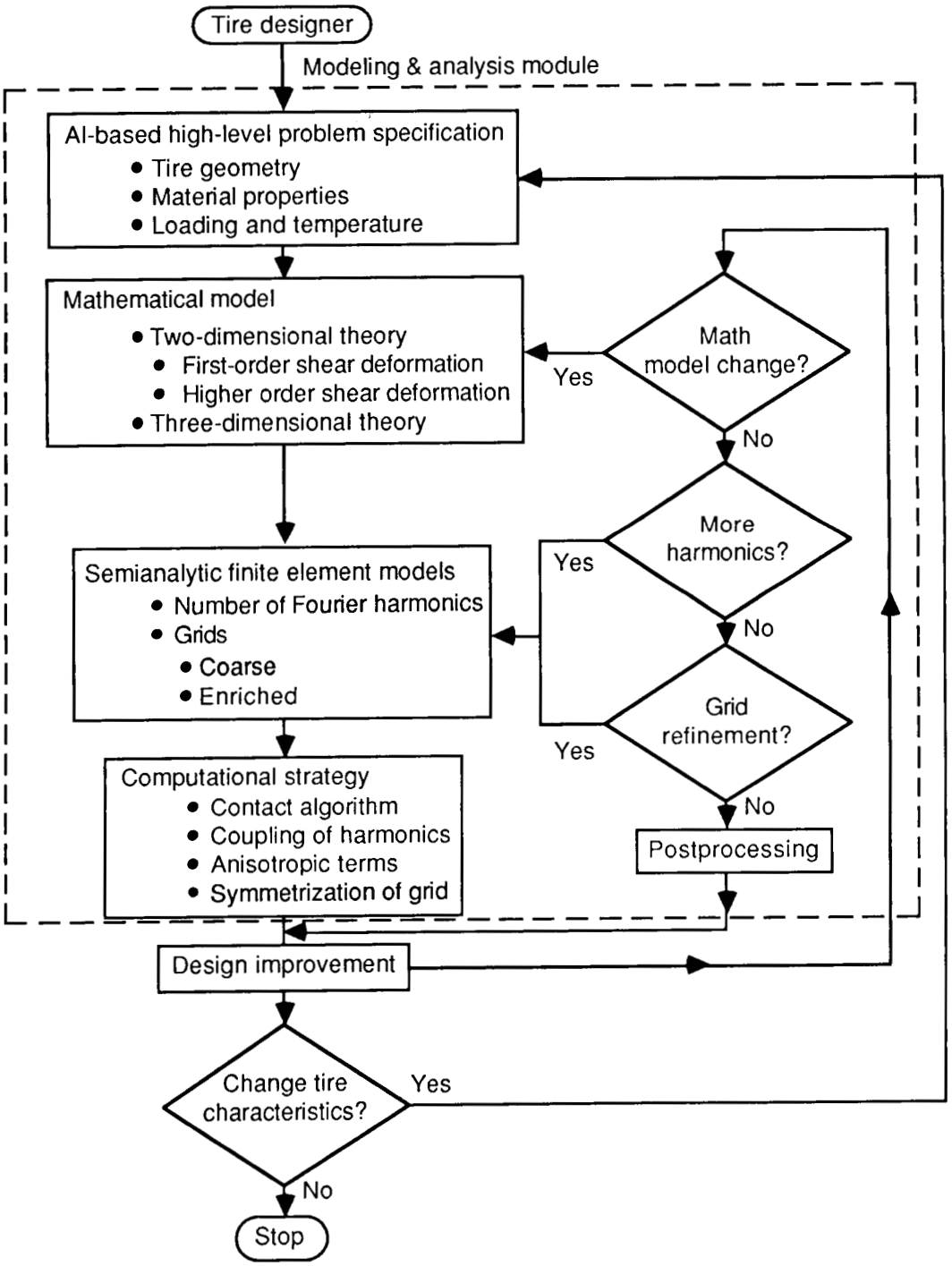

Figure 1. Schematic of the tire design process.

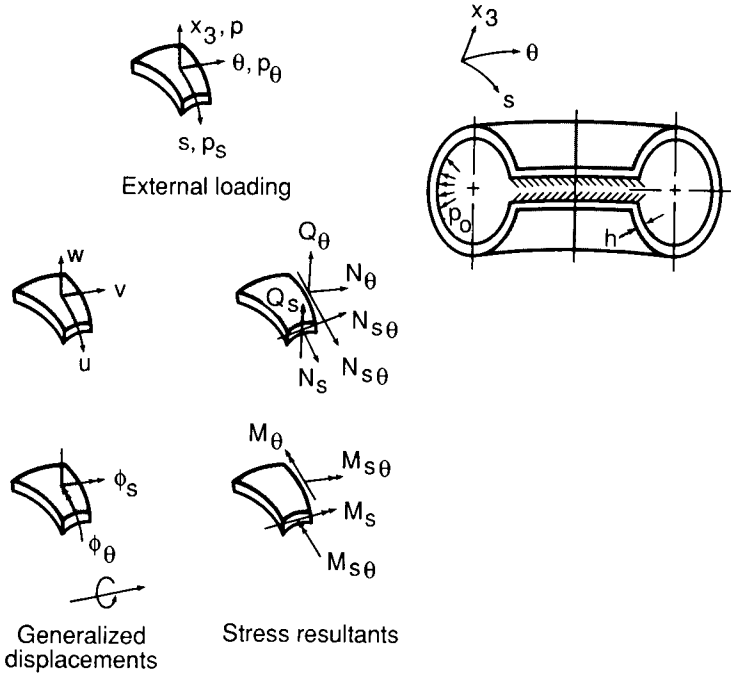

Figure 2. Tire model and sign convention of stress resultants, generalized displacements, and external loading.

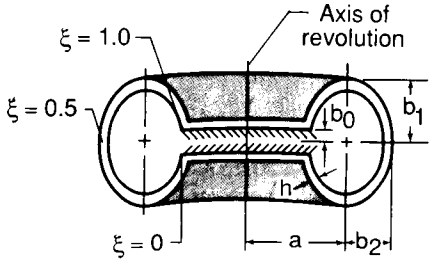

Boundary conditions:
At $\xi = 0$

$u = \bar{v} = w = \phi_s = \bar{\phi}_\theta = 0$

$\bar{u} = v = \bar{w} = \bar{\phi}_s = \phi_\theta = 0$

At $\xi = 0.5$

Symmetry condition

$u = \phi_s = v = \bar{w} = \phi_\theta = 0$

Antisymmetry condition

$\bar{u} = \bar{\phi}_s = \bar{v} = w = \bar{\phi}_\theta = 0$

E_L = 517 MPa

E_T = 8.27 MPa

G_{LT} = 3.10 MPa

G_{TT} = 1.86 MPa

ν_{LT} = 0.4

h = 1.067 cm

b_0 = 5.08 cm

b_1 = 6.223 cm

b_2 = 5.385 cm

a = 19.558 cm

Number of layers = 2

Fiber orientation: [+55°/-55°]

Figure 3. Two-layered anisotropic tire used in the present study.

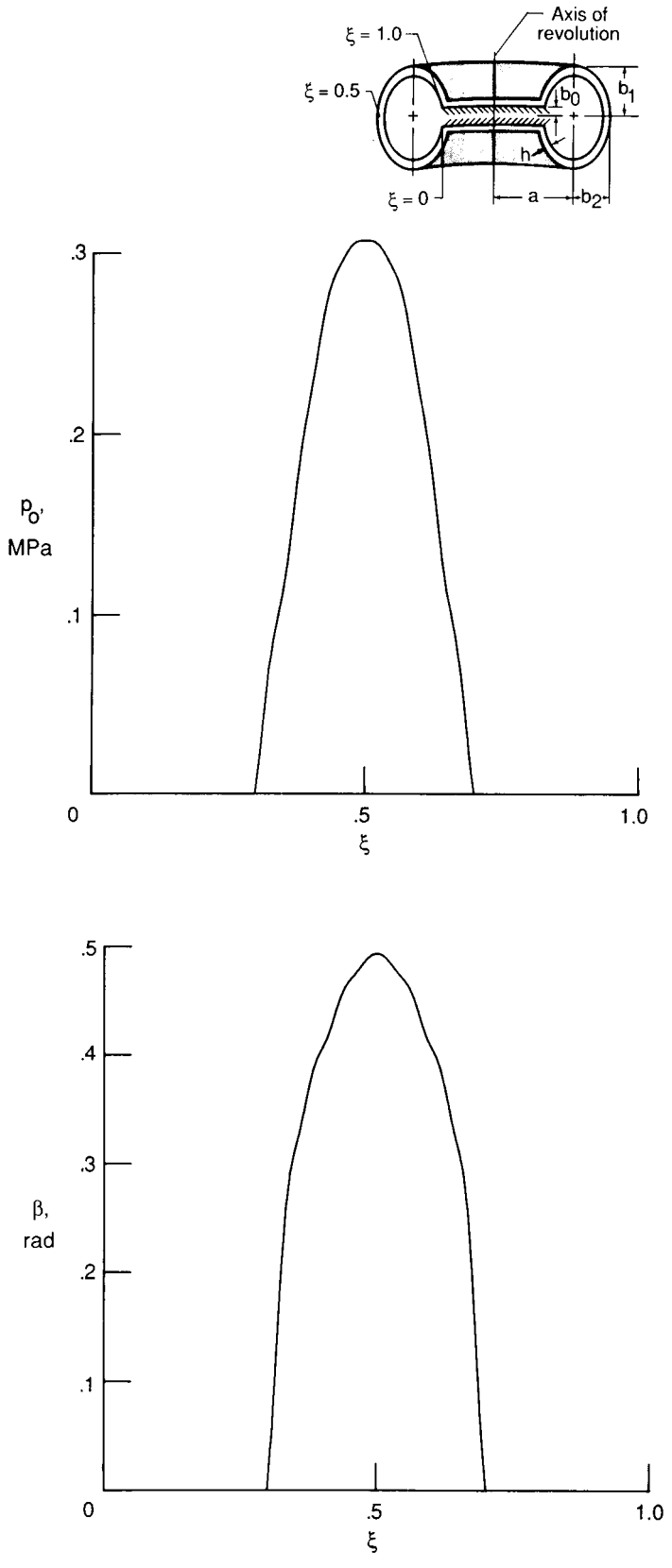

Figure 4. Variation of contact pressure and contact angle in the meridional direction.

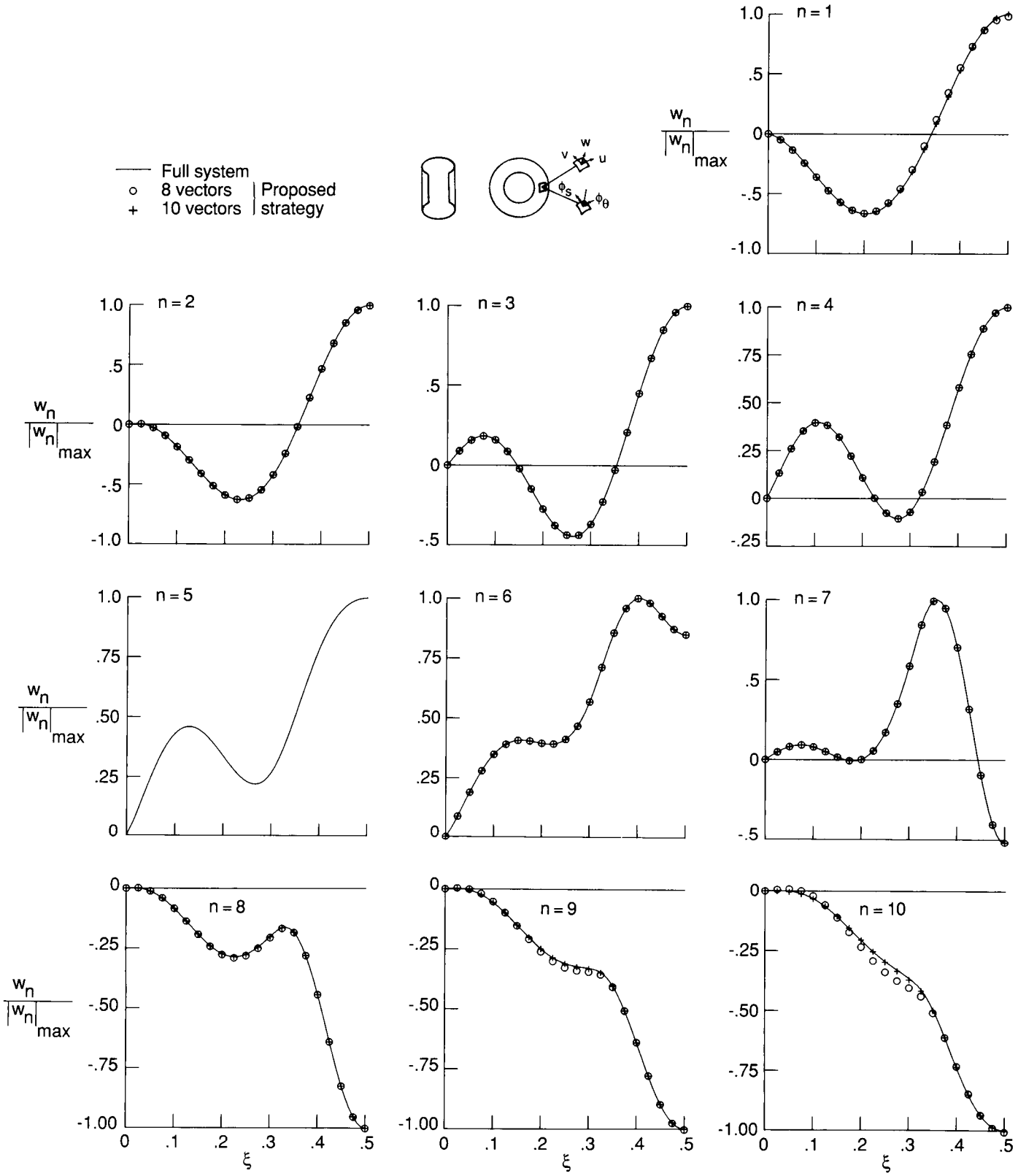

Figure 5. Accuracy of transverse displacements w_n obtained by the proposed procedure. Two-layered anisotropic tire shown in figure 3; $n_o = 5$.

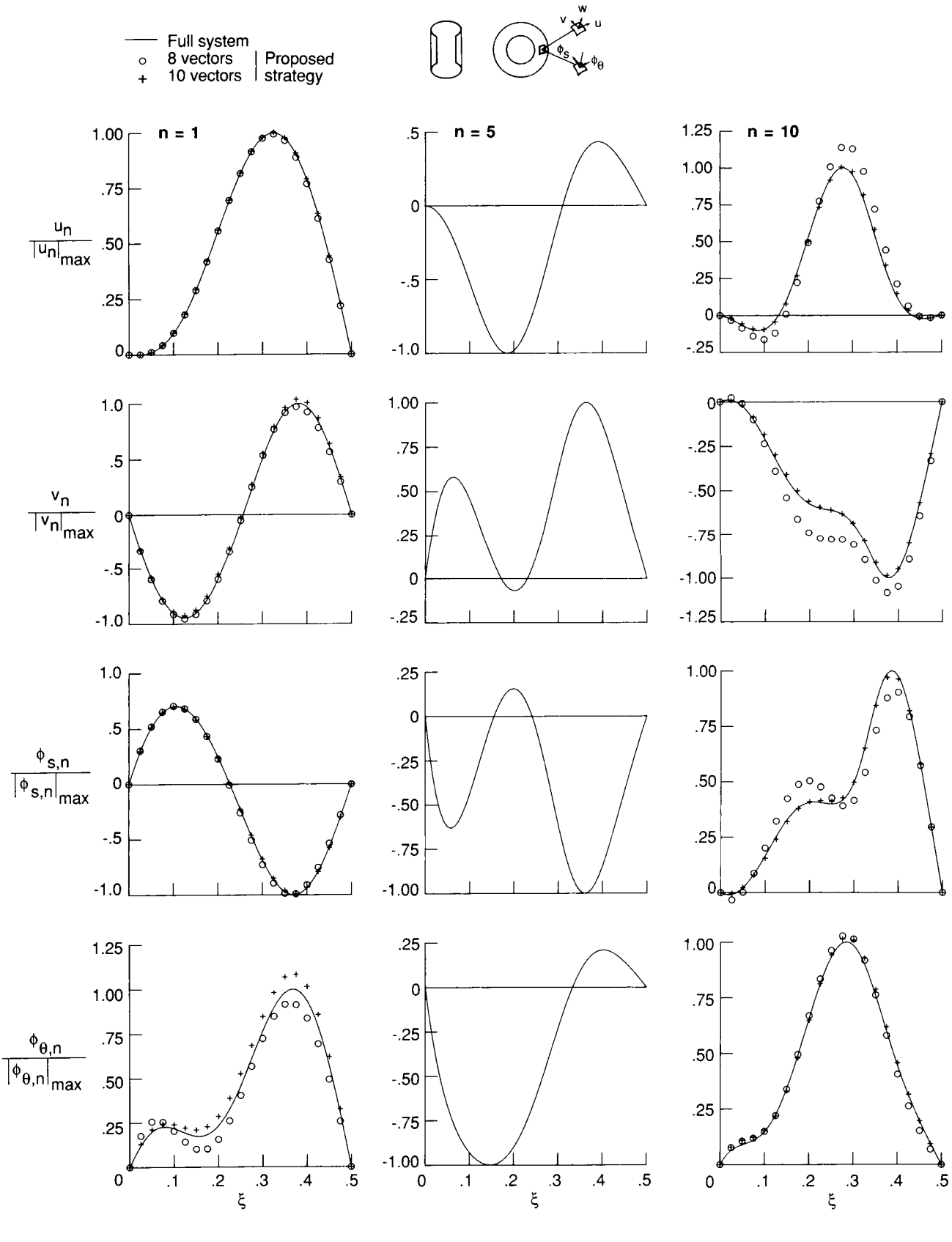

Figure 6. Accuracy of in-plane displacements and rotation components obtained by the proposed procedure. Two-layered anisotropic tire shown in figure 3; $n_o = 5$.

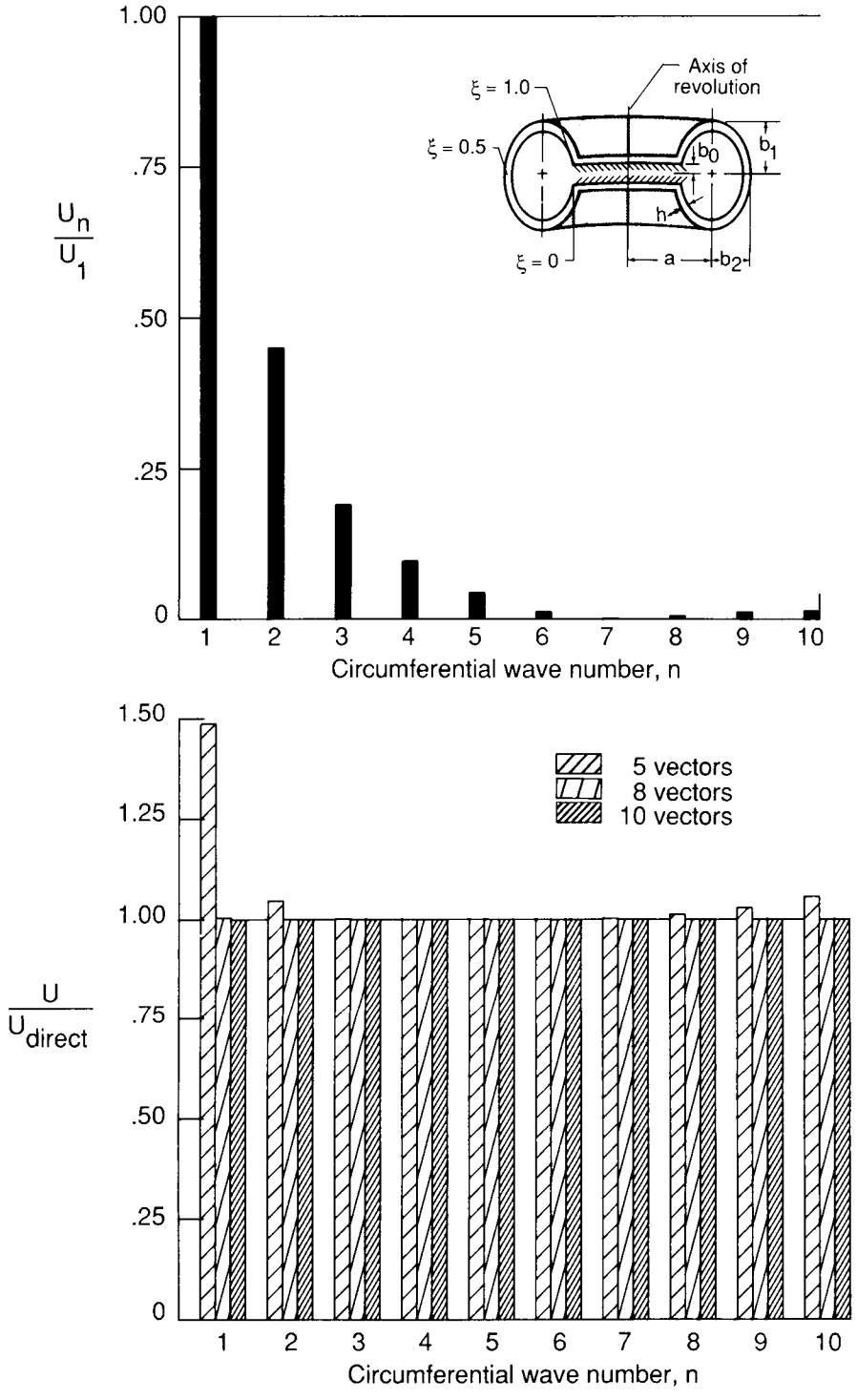

Figure 7. Accuracy of total strain energy of the shell obtained by the proposed procedure. Two-layered anisotropic tire shown in figure 3.

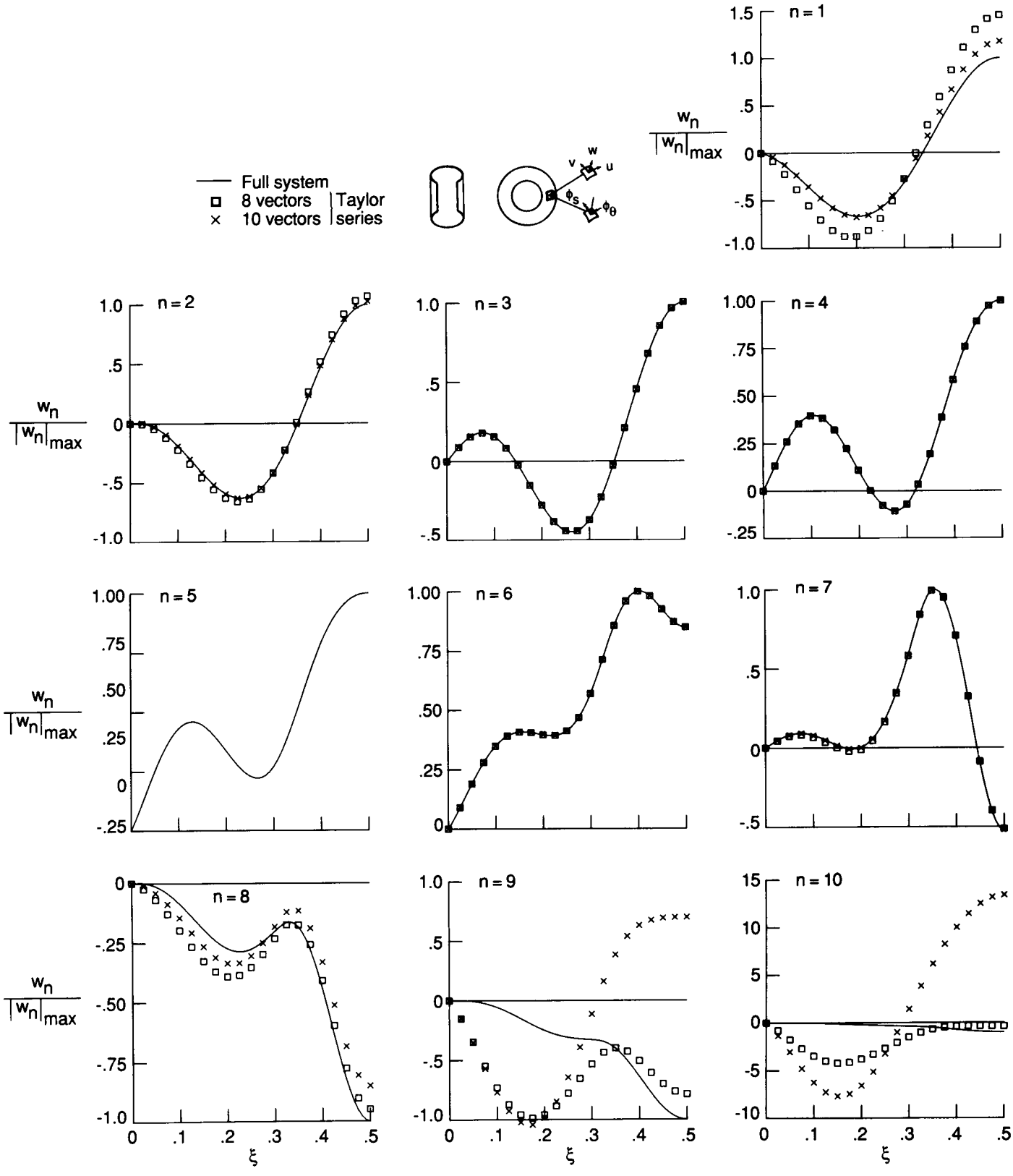

Figure 8. Accuracy of normal displacement w_n obtained by Taylor series expansion at $n_o = 5$. Two-layered anisotropic tire shown in figure 3.

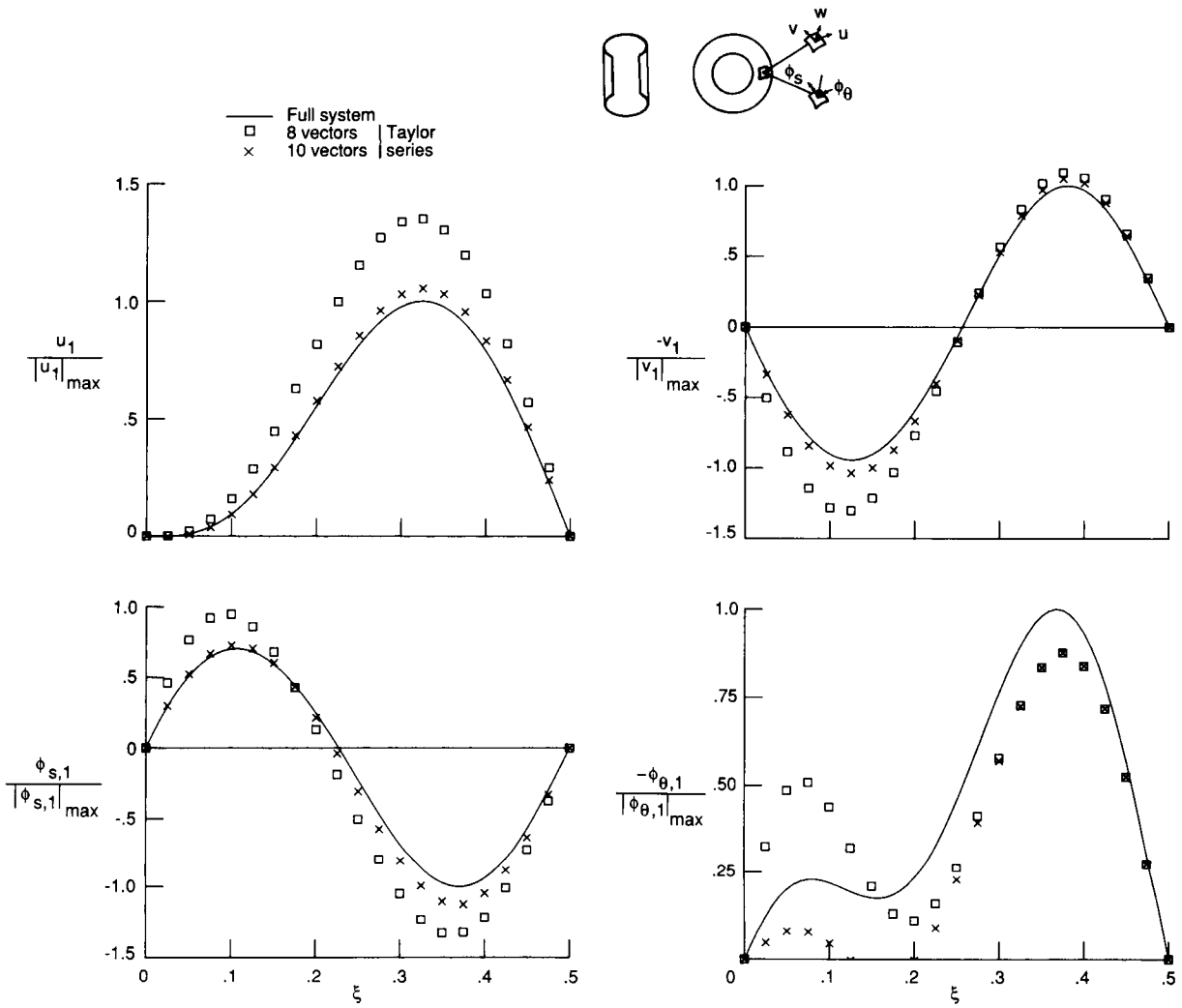

Figure 9. Accuracy of in-plane displacements and rotation components obtained by Taylor series expansion at $n_o = 5$. Two-layered anisotropic tire shown in figure 3.

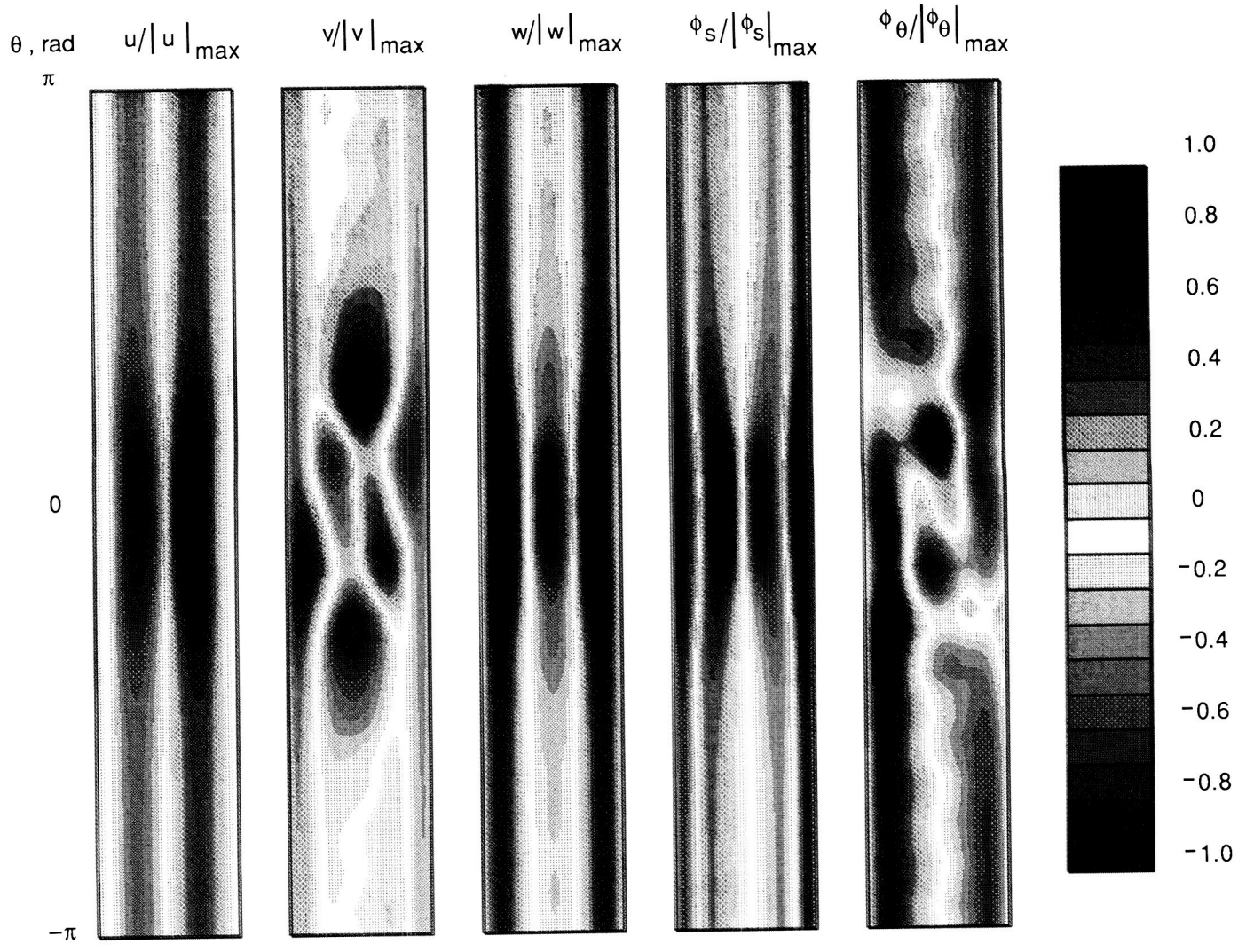

Figure 10. Normalized contour plots for the generalized displacements. Two-layered anisotropic tire subjected to combined inflation pressure and localized loading (see fig. 3). The range of the contours is -1.0 to $+1.0$ at increments of 0.1.

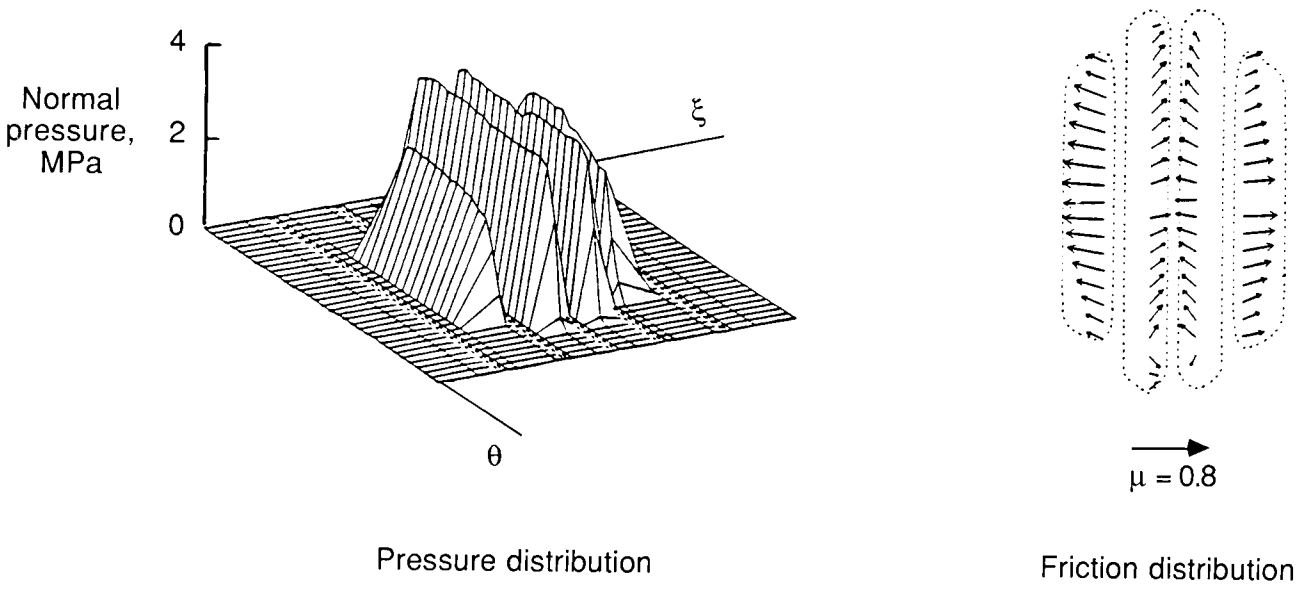

Figure 11. Measured pressure and friction distribution in contact area of Space Shuttle orbiter nose gear tire under static loading conditions. Vertical load, 67 kN; inflation pressure, 2.17 MPa.

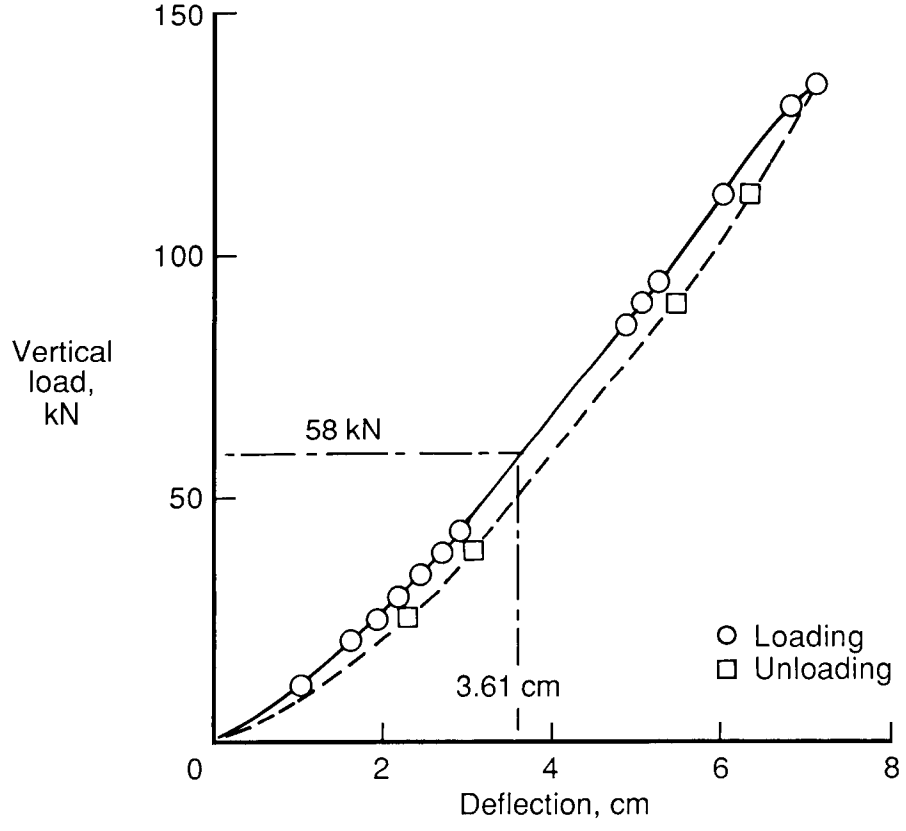

Figure 12. Load-deflection curve for Space Shuttle orbiter nose gear tire subjected to static vertical loading on a flat surface. Inflation pressure, 2.17 MPa.

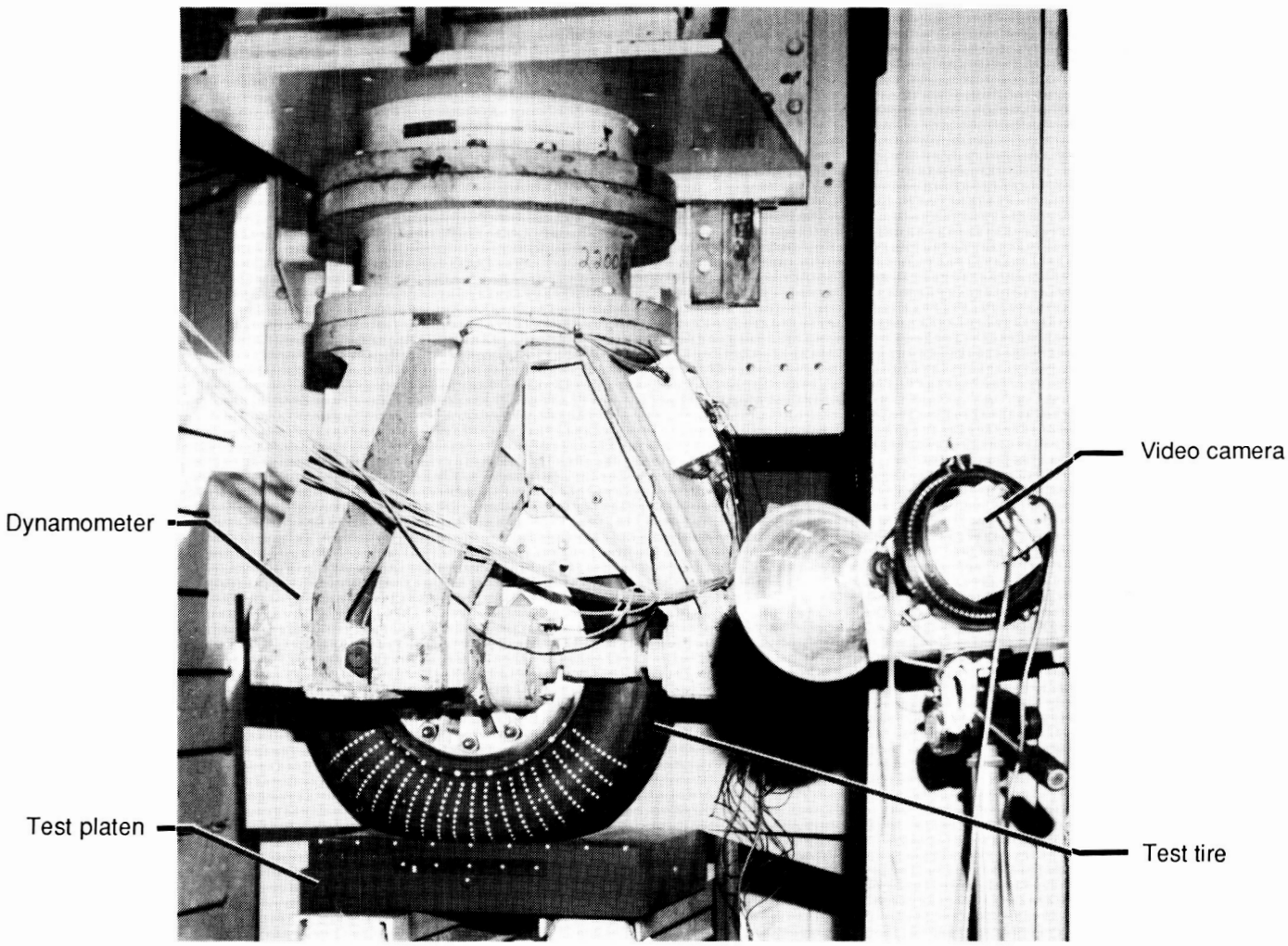

L-85-12753

Figure 13. Experimental arrangement for close-range photogrammetry measurements of tire sidewall deformations.

ORIGINAL PAGE
COLOR PHOTOGRAPH

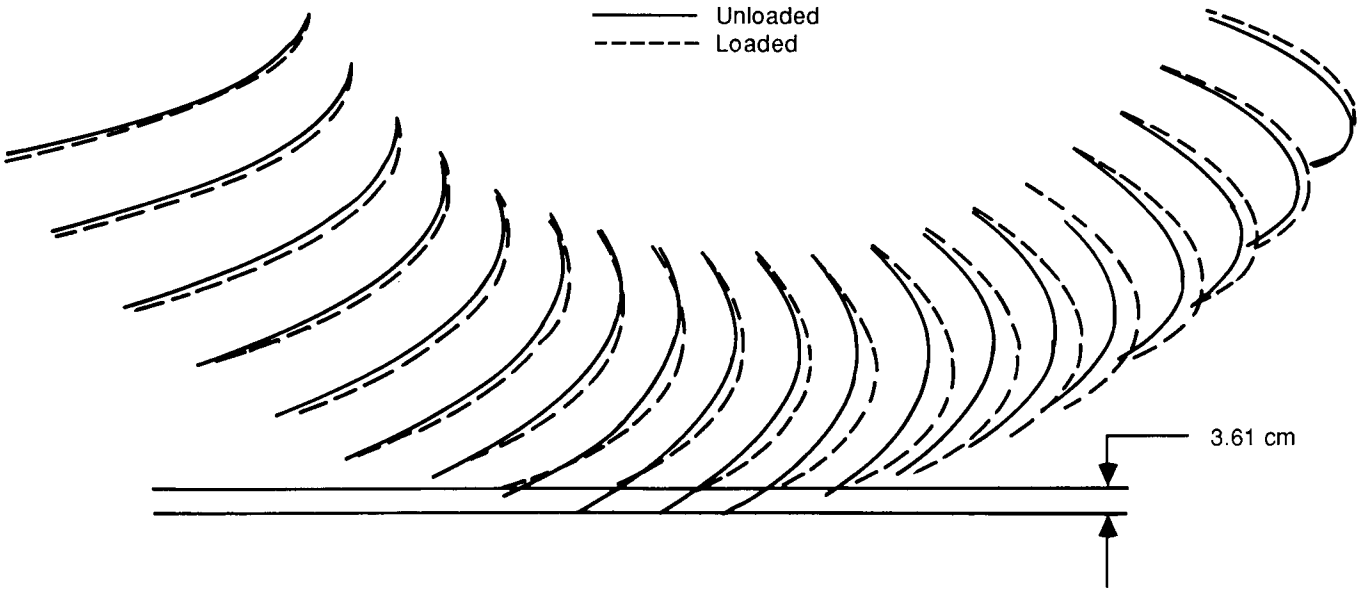

Figure 14. Three-dimensional representation of Space Shuttle orbiter nose gear tire sidewall deformations based on close-range photogrammetry data.

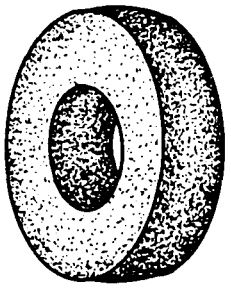

(a) Inflation pressure.

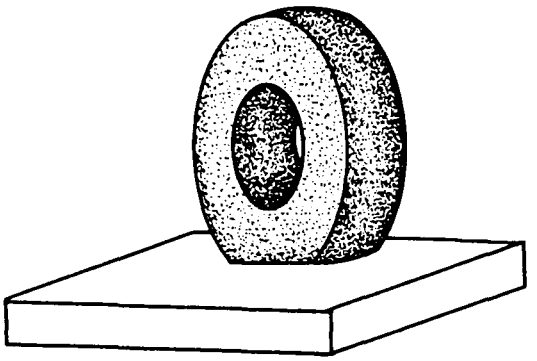

(b) Inflation pressure and static vertical loading.

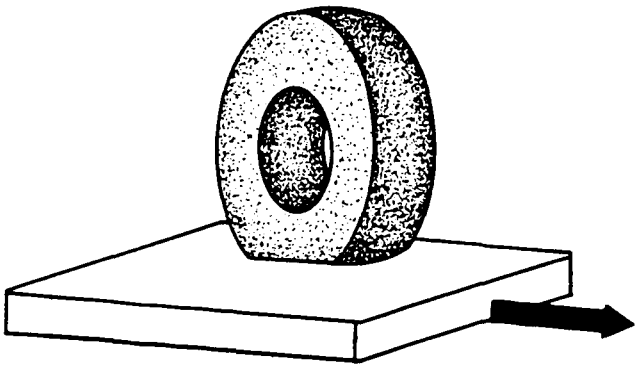

(c) Inflation pressure, static vertical loading, and externally applied drag load.

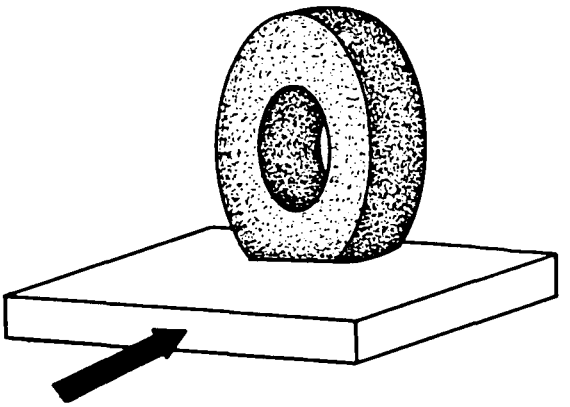

(d) Inflation pressure, static vertical loading, and externally applied lateral load.

Figure 15. Loading conditions for the initial set of benchmark problems from the National Tire Modeling Program.

NASA
National Aeronautics and Space Administration

Report Documentation Page

1. Report No.	2. Government Accession No.	3. Recipient's Catalog No.
NASA TP-2781		

4. Title and Subtitle	5. Report Date
Advances in Contact Algorithms and Their Application to Tires	April 1988
	6. Performing Organization Code
7. Author(s)	8. Performing Organization Report No.
Ahmed K. Noor and John A. Tanner	L-16376
	10. Work Unit No.
9. Performing Organization Name and Address	505-63-41-02
NASA Langley Research Center Hampton, VA 23665-5225	11. Contract or Grant No.
	13. Type of Report and Period Covered
12. Sponsoring Agency Name and Address	Technical Paper
National Aeronautics and Space Administration Washington, DC 20546-0001	14. Sponsoring Agency Code

15. Supplementary Notes

Presented at the 1987 American Chemical Society Meeting in Montreal, Quebec, Canada, May 26–29, 1987.

Ahmed K. Noor: The George Washington University, Joint Institute for Advancement of Flight Sciences, Langley Research Center, Hampton, Virginia.
John A. Tanner: Langley Research Center, Hampton, Virginia.

16. Abstract

Currently used techniques for tire contact analysis are reviewed. Discussion focuses on the different techniques used in modeling frictional forces and the treatment of contact conditions. A status report is presented on a new computational strategy for the modeling and analysis of tires including solution of the contact problem. The strategy is based on solving the complex tire contact problem as a sequence of simpler problems and obtaining information about the sensitivity of the tire response to each of the complicating factors. The key elements of the proposed strategy are (1) use of semianalytic mixed finite elements in which the shell variables are represented by Fourier series in the circumferential direction and piecewise polynomials in the meridional direction, (2) use of perturbed Lagrangian formulation for the determination of the contact area and pressure, (3) application of multilevel operator splitting to effect successive simplification of the governing equations, and (4) application of multilevel iterative procedures and reduction techniques to generate the response of the tire. Numerical results are presented to demonstrate the effectiveness of a proposed procedure for generating the tire response associated with different Fourier harmonics.

17. Key Words (Suggested by Authors(s))	18. Distribution Statement
Tire modeling Contact problems Operator splitting Friction laws Benchmark problems	Unclassified –Unlimited Subject Category 39

19. Security Classif.(of this report)	20. Security Classif.(of this page)	21. No. of Pages	22. Price
Unclassified	Unclassified	35	A03

For sale by the National Technical Information Service, Springfield, Virginia 22161-2171